SSRG International Journal of Civil Engineering
ISSN: 2348-8352/ https://doi.org/10.14445/23488352/IJCE-V13I11P113

Volume 13 Issue 11, 225-252, November 2026
© 2026 Seventh Sense Research Group®

Original Article

Assessment of Groundwater Quality and Contamination Sources in the Jojari River Watershed, Jodhpur District (Arid Zone, Rajasthan): A Tributary of the Luni River Basin, India

Umesh Kumar[1], Suresh Kumar Singh[2]

[1,2]*Department of Civil Engineering, MBM University, Jodhpur, Rajasthan, India.*

[1]*Corresponding Author: umesh.ce@mbm.ac.in*

Received: 17 August 2026 Revised: 29 October 2026 Accepted: 12 November 2026 Published: 27 November 2026

Abstract *- Groundwater is the main source of drinking and irrigation water in the arid Jojari River watershed, a tributary of the Luni River in Jodhpur district, Rajasthan, India. Four industrial areas (Basni, Sangaria, Salawas and Boranada) within the watershed have discharged effluent into the Jojari channel for decades. This study assesses agency groundwater quality records for 59 wells from the April- May 2025 pre-monsoon season. A weighted Water Quality Index (WQI), irrigation indices, Piper and Gibbs diagrams, Principal Component Analysis (PCA) and Hierarchical Cluster Analysis (HCA) are combined with a GIS-based proximity test against mapped industrial-area boundaries, with sensitivity checks. Electrical Conductivity (EC) ranges from 530 to 23,194 µS/cm, and 88.1% of wells are Poor to Unsuitable for drinking, a share robust to alternative WQI weights and a ±5% charge-balance limit. Na-Cl water forms about 85% of samples, and evaporation is the main natural control. Three components (74.7% of variance) represent salinity, geogenic fluoride and nitrate. EC, Total Dissolved Solids (TDS), Na^+, Cl^- and SO_4^{2-} decrease with distance from the industrial corridor ($p \leq 0.020$), nitrate increases slightly, and fluoride shows no trend. The salinity association weakens without four extreme wells and overlaps the regional salinity gradient. It is strongest in Luni block, which holds all 11 wells within 3 km of the industrial areas; these have 2.0-2.9 times higher EC, TDS and sulphate than other Luni wells. Industrial influence on Luni block is therefore probable but unconfirmed, and tracer-based monitoring should focus there.*

Keywords *- GIS proximity analysis, Groundwater quality, Industrial wastewater, Principal component analysis, Water Quality Index.*

1. Introduction

In arid and semi-arid regions, groundwater is often the only dependable source of water for drinking, domestic use and farming. Western Rajasthan is a clear example. Annual rainfall seldom exceeds 300–400 mm and varies widely from year to year, so towns and irrigated farms draw almost all of their water from alluvial and hard-rock aquifers. High evapotranspiration, weak natural recharge, heavy pumping and the spread of urban and industrial land over shallow aquifers make this groundwater vulnerable both to natural salinisation and to pollution from human activity [1, 2].

The Jojari River watershed in Jodhpur district shows these pressures in an acute form. The Jojari is a seasonal tributary of the Luni River that drains Jodhpur city and its industrial fringe. Four notified industrial areas, Basni, Sangaria, Salawas and Boranada, sit inside the watershed. Many of their units are textile dyeing and printing works, and their effluent, together with the sewage of Jodhpur city, has reached the Jojari channel for decades [3, 4]. Yet there is little watershed-scale evidence on how far this effluent has affected the groundwater that villages along the river still drink.

Three gaps stand out in the existing work, which is reviewed in Section 2. First, groundwater studies in and around Jodhpur have been local, have covered only a few parameters, or have been descriptive, and none has examined the whole Jojari watershed with a full major-ion data set. Second, studies in Rajasthan that use WQI and multivariate statistics usually attribute high salinity to "natural and anthropogenic sources" without testing which source dominates at which wells. Third, where groundwater chemistry has been related to industrial location, the link has rested on map overlays or on a single correlation, and its sensitivity to extreme values and to regional trends has seldom been examined. As a result, it is still unclear how much of the

This is an open access article under the CC BY-NC-ND license (http://creativecommons.org/licenses/by-nc-nd/4.0/)

extreme salinity in the lower Jojari watershed comes from evaporation in an arid aquifer and how much may be added by industrial wastewater.

The present study addresses these gaps with data from 59 wells sampled in the 2025 pre-monsoon season. Its specific objectives are to:

(a) Characterise the physicochemical composition of groundwater in the Luni, Mandore, Baori and Tinwari blocks of the watershed;
(b) Assess drinking-water suitability with a weighted arithmetic Water Quality Index (WQI) based mainly on BIS IS 10500:2012 [5], with stated reference values for Electrical Conductivity (EC) and sodium;
(c) Assess irrigation suitability with the Sodium Adsorption Ratio (SAR), percent sodium (%Na), Residual Sodium Carbonate (RSC) and the United States Salinity Laboratory (USSL) classification;
(d) Identify hydrochemical facies and the main geochemical controls with Piper [6] and Gibbs [7] diagrams;
(e) Apply Pearson correlation, Principal Component Analysis (PCA) and Hierarchical Cluster Analysis (HCA) to group wells for geogenic and anthropogenic sources; and
(f) Map the main parameters with a Geographic Information System (GIS) and test statistically how they change with distance from the four industrial areas.

The methodological contribution lies in objective (f), and it needs to be stated carefully, because distance correlation and buffer analysis are established tools [8, 9]. What is new here is the way they are used. First, distance is measured to the mapped boundary polygons of the industrial areas rather than to point locations. Second, the distance test is used to check the PCA and HCA source signals against each other, since an industrial salinity source, a geogenic fluoride source and a diffuse nitrate source should each behave differently with distance. Third, the association is subjected to a fixed set of robustness checks: rank-based tests, three buffer widths, removal of the most extreme wells, control for regional position, and a within-block test. These checks decide how far the association can be read as evidence of industrial influence. The results also provide a watershed-wide baseline for the Jojari, against which future remediation can be judged.

2. Review of Literature

2.1. Index-based and Multivariate Assessment in Rajasthan and India

Water quality indices combined with multivariate statistics are now the standard tools for regional groundwater assessment in India. In the semi-arid Ayad river basin near Udaipur, a weighted arithmetic WQI computed from Ground Water Department and CGWB records for 2000–2023 showed quality worsening from west to east, with salinity the main problem in the eastern part of the basin [10]. Gautam et al. [11] combined an integrated WQI with PCA and cluster analysis to separate rock–water interaction from human inputs, and Choudhary et al. [12] used graphical, multivariate and index methods to rank natural and anthropogenic sources and the health risks they pose in another part of Rajasthan. In a hard-rock aquifer of the state, Machiwal and Jha [13] paired multivariate statistics with geostatistical mapping to locate sources of contamination. Bhakar and Singh [14] applied PCA and HCA to 43 samples from a hyper-arid part of Rajasthan, a setting close to that of the present study. Studies outside Rajasthan follow the same pattern. Geogenic controls on drinking-water quality were examined in semi-arid Mahendragarh, Haryana [15]; WQI, PCA and the Piper, Wilcox and USSL diagrams showed many unsafe wells and a fluoride problem in Nalanda, Bihar [16]; GIS-based WQI mapping marked zones for action in Natham Taluk, Tamil Nadu [17, 18]; and Piper facies with correlation and cluster analysis separated mineral weathering from evaporation and human inputs in hard-rock Perambalur [19]. Nemerow's pollution index has also been used to find small contamination hotspots in the groundwater critical zone of western Rajasthan [20].

2.2. Nitrate and Fluoride in Semi-Arid Aquifers

Nitrate and fluoride are the two health-related contaminants most often reported from Rajasthan. Suthar et al. [2] found nitrate above the drinking limit in many rural villages of the state and linked it to fertilizer use and animal and human waste. In Dausa district, Rahman et al. [21] estimated a natural nitrate background of 7.2 mg/L and found that 28% of samples exceeded the BIS limit of 45 mg/L. Mondal et al. [1] reported nitrate up to 491.6 mg/L and fluoride up to 6.50 mg/L in a semi-arid part of Rajasthan, with about 26% of samples above 1.5 mg/L of fluoride and chemical weathering as the main control. These studies show that nitrate and fluoride usually come from sources different from those of salinity, which is why they need to be treated separately in source screening.

2.3. Industrial Effluent and Groundwater in the Luni Basin

Textile processing uses large amounts of sodium chloride and sodium sulphate as electrolytes in reactive dyeing, and its effluent is saline, coloured and high in dissolved solids [22, 23]. In the Luni basin, the best-documented case is Pali, where Bhadra et al. [24] used field and satellite data to trace the impact of textile effluent on groundwater around the city, and Pathak et al. [25] found that nitrate, fluoride and heavy metals in wells along the Bandi River rose between 1998 and 2009. For Jodhpur, a pollution abatement action plan was prepared after the city was listed as a Critically Polluted Industrial Cluster [3], a review has summarised industrial wastewater practice and its effects across western Rajasthan [4], and two-dimensional hydrodynamic modelling has described flow, flooding and human influence on the Jojari channel for 2015–2020 [26]. None of these studies, however, measured groundwater chemistry across the whole Jojari watershed or tested it against the location of the industrial areas.

2.4. Source Apportionment and Spatial Methods

Recent studies have moved from naming likely sources to estimating their shares. Bhagwat and Ojha [27] used an ensemble of HCA, PCA and Positive Matrix Factorisation (PMF) in the Hindon–Yamuna interbasin, and Li et al. [28] used a PCA–PMF–Mantel framework in the Qujiang River Basin, China. Such methods generally require large data sets, preferably covering several seasons, and ideally source profiles or tracers. On the spatial side, Inverse Distance Weighting (IDW) and kriging are among the most widely used methods for mapping groundwater quality. Comparative work has found that neither is always better and that the choice depends on sample density, data distribution and the purpose of the map [29, 30].

2.5. Industrial Proximity in Groundwater Studies

Several studies have linked groundwater quality to nearby industry, but the link has usually rested on location rather than on a formal test. Krishna et al. [31] applied PCA and HCA to 120 wells around the Katedan industrial area near Hyderabad and attributed As, Cr, Cd, Ni, Pb and Zn to industrial effluent, without examining how concentrations changed with distance. Yadav et al. [32] combined PCA with IDW mapping in Agra, where about 7,200 small industrial units operate, and still identified rock weathering as the main control on groundwater chemistry. Zamani et al. [8] did include distance to a lead–zinc plant in their correlation matrix; the correlations were weak and not significant, yet the plant was named as a main source on the basis of metal–metal associations. More recently, Alagulakshmi et al. [9] used buffers and nearest-neighbour distances around industries and quarries in the Muvattupuzha basin together with PCA and an entropy-weighted index, but with only 15 wells. Distance and buffer analysis are therefore established tools. What these studies generally do not report is whether the association survives rank-based testing, removal of extreme wells and control for regional trends, and without these checks a screening signal can easily be over-stated as source attribution.

2.6. Research Gap

The review shows that (i) the Jojari watershed has no published watershed-scale hydrochemical assessment with a full major-ion suite; (ii) source attribution in most Indian WQI and PCA studies remains qualitative; and (iii) where distance to industry has been tested, the robustness of the association to extreme values, regional trends and the choice of buffer has rarely been reported, so a screening signal is easily read as confirmed contamination. The present study is designed to address these three gaps.

3. Study Area

The Jojari is a seasonal, monsoon-fed stream that runs south-west through Jodhpur district and joins the Luni River, the main river of western Rajasthan, which ends in the Rann of Kachchh without reaching the sea [26]. The watershed studied here lies wholly within Jodhpur district and covers parts of four blocks (Luni, Mandore, Baori and Tinwari), with urban fringe, industrial and rural farmland. The delineated watershed covers about 1,754 km², so the 59 wells give an average density of about one well per 30 km². The climate is arid to semi-arid. Mean annual rainfall is generally below 350 mm, falls mostly during the south-west monsoon (July-September), and is far exceeded by potential evapotranspiration for most of the year. Groundwater occurs in shallow to moderately deep unconfined and semi-confined aquifers in Quaternary alluvium, windblown sand, sandstone and weathered or fractured granite and rhyolite. Recharge comes mainly from monsoon infiltration and, locally, from irrigation return flow and seepage of urban and industrial wastewater.

The four industrial areas host textile dyeing, handicraft processing, chemical and allied small and medium units typical of the region [4], and together they form part of the Jodhpur Critically Polluted Industrial Cluster [3]. For decades, the Jojari and its drains have carried treated and, at times, poorly treated effluent, along with domestic sewage from Jodhpur city. An evaporative climate, saline and fluoride-prone rocks and concentrated effluent loading together make the watershed a complex system in which both natural and human processes shape groundwater chemistry.

Groundwater-quality records for 59 wells, sampled in April and May 2025 (pre-monsoon), were compiled from the Ground Water Department (GWD), Rajasthan, the Central Ground Water Board (CGWB) and the Rajasthan State Pollution Control Board (RSPCB). Of these, 28 wells are in Luni block, 21 in Mandore, 6 in Baori and 4 in Tinwari. Figure 1 shows the location of the watershed from national to local scale, and Figure 2 shows the stream network, industrial areas and wells.

The distribution of wells follows the agency monitoring networks rather than a design made for this study. Coverage is densest in Luni block, which contains the industrial corridor and the downstream part of the watershed where both evaporative salinity and effluent inputs are expected to accumulate, and sparsest in the upper Baori and Tinwari blocks. Over the 1,754 km² watershed, the average density is one well per 30 km², and the mean nearest-neighbour distance is 3.6 km (median 3.4 km, maximum 8.3 km). The Clark–Evans ratio of 1.30 [33] indicates that the wells are, if anything, more evenly spaced than a random pattern at the watershed scale, so the network is not clustered in one area.

The network is adequate for watershed-level patterns and for the Luni and Mandore blocks, but block-level results for Baori (n = 6) and Tinwari (n = 4) are less certain. To check that the watershed-level result is not driven by the dense Luni coverage, the share of Poor to Unsuitable wells was also computed with each block weighted equally; it is 82.1%, close to the 88.1% obtained with all wells pooled.

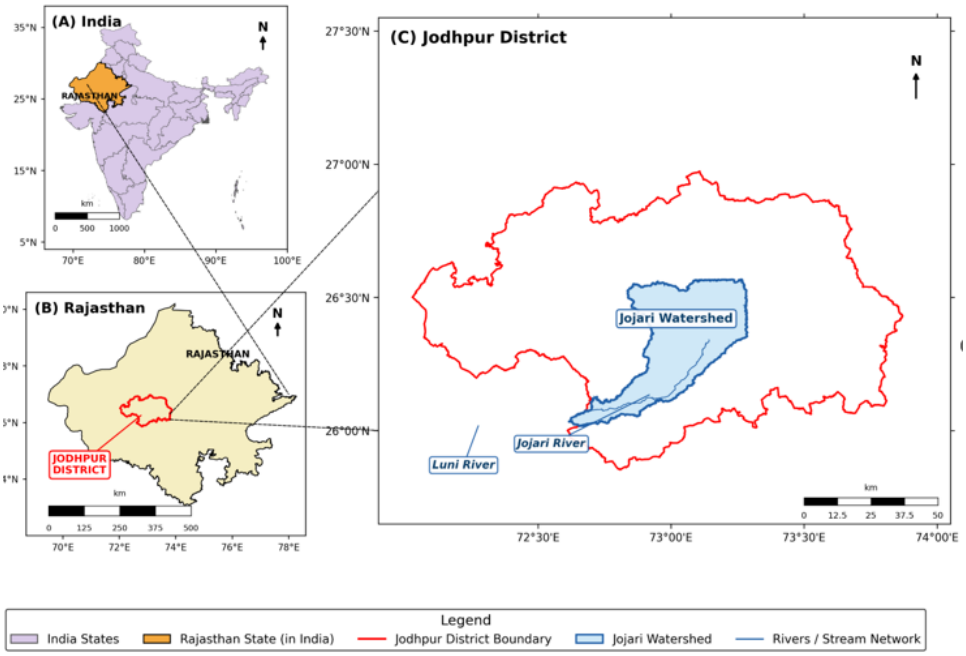


Fig. 1 Location and index map of the Jojari River watershed within Jodhpur District, Rajasthan, India

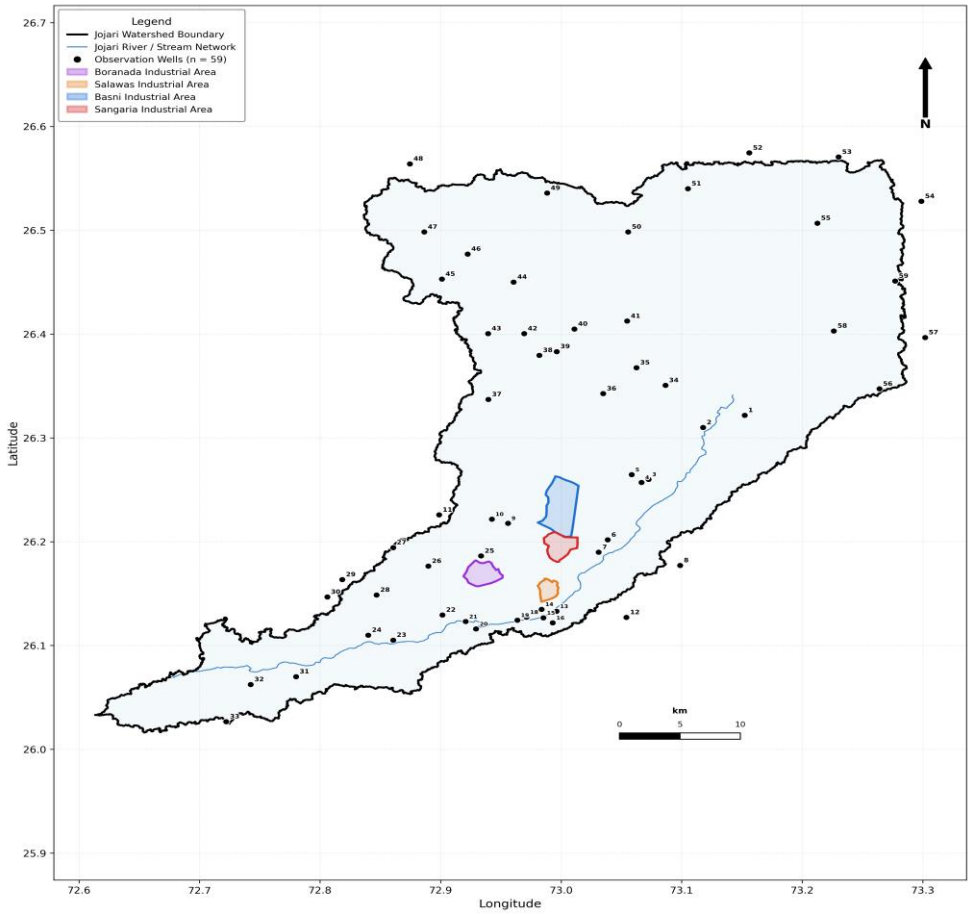


Fig. 2 Jojari river watershed showing stream network, industrial areas and groundwater monitoring locations

Figure 3 shows the main aquifer systems. Granite and related acidic crystalline rocks (pegmatite, granite, syenite and rhyolite) underlie most of the watershed, including Luni block and all four industrial areas. A broken belt of sandstone with shale occupies the north (Mandore and northern Baori), and a small outcrop of shale with sandstone lies in the far north-east. This crystalline geology is a likely source of geogenic fluoride, which is discussed in Sections 5.1, 5.7, 5.8 and 5.9.

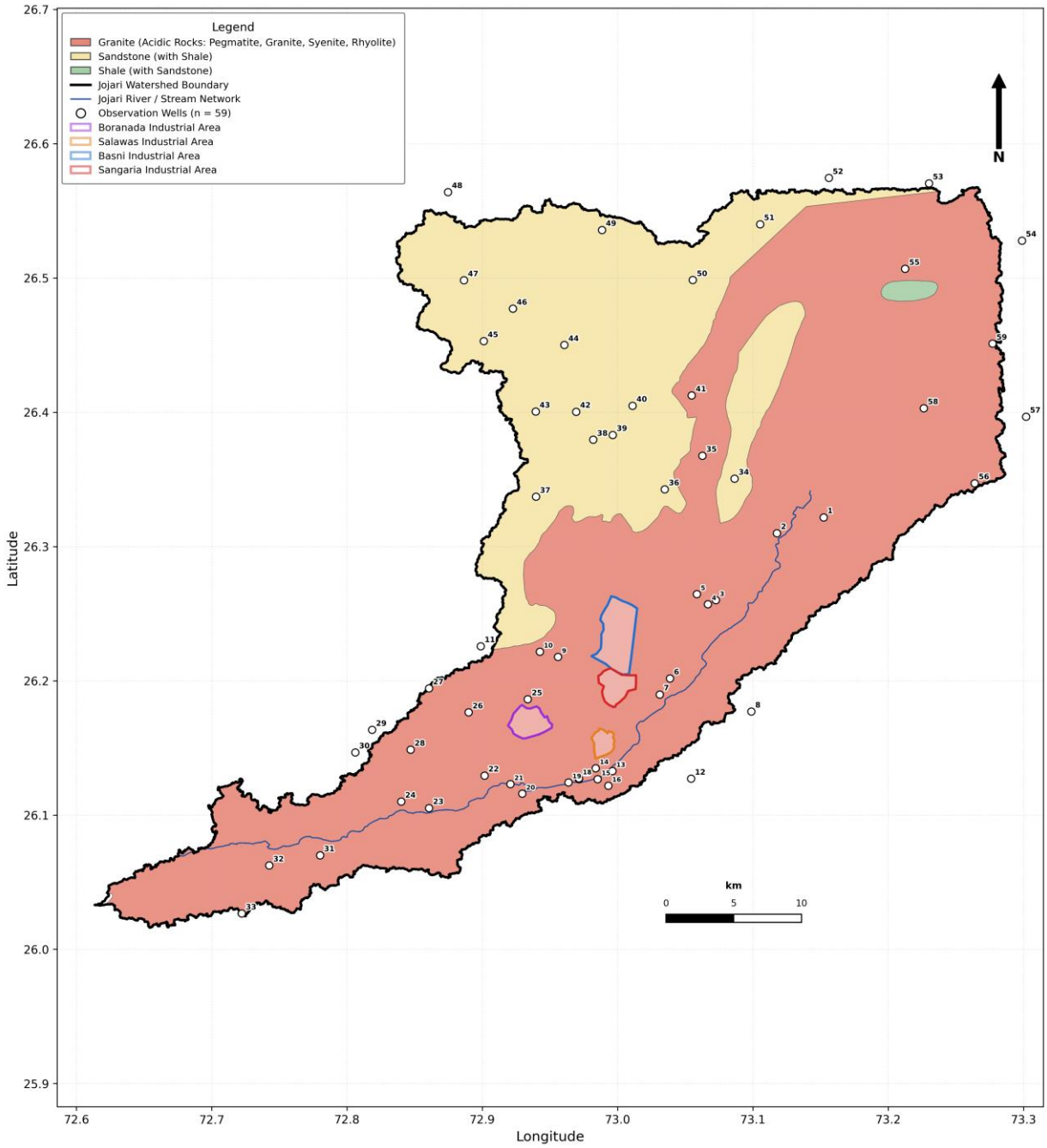


Fig. 3 Geological map of the Jojari River watershed showing principal aquifer systems

Figure 4 shows the water-table elevation, which ranges from about 83 to 198 m above mean sea level. The highest values (above 180 m) occur in a west-central zone around Mandore block (near wells 36-41) and in the far north-east. The lowest occur at the far north-west (around well 47) and, most clearly, in the far south-west near the outlet (well 33, about 83 m). The head therefore falls from the interior towards the south-western outlet, in line with the drainage direction of the Jojari. This suggests a regional groundwater flow towards the south-west, where both evaporative salinity and effluent inputs would be expected to build up (Sections 5.2 and 5.9).

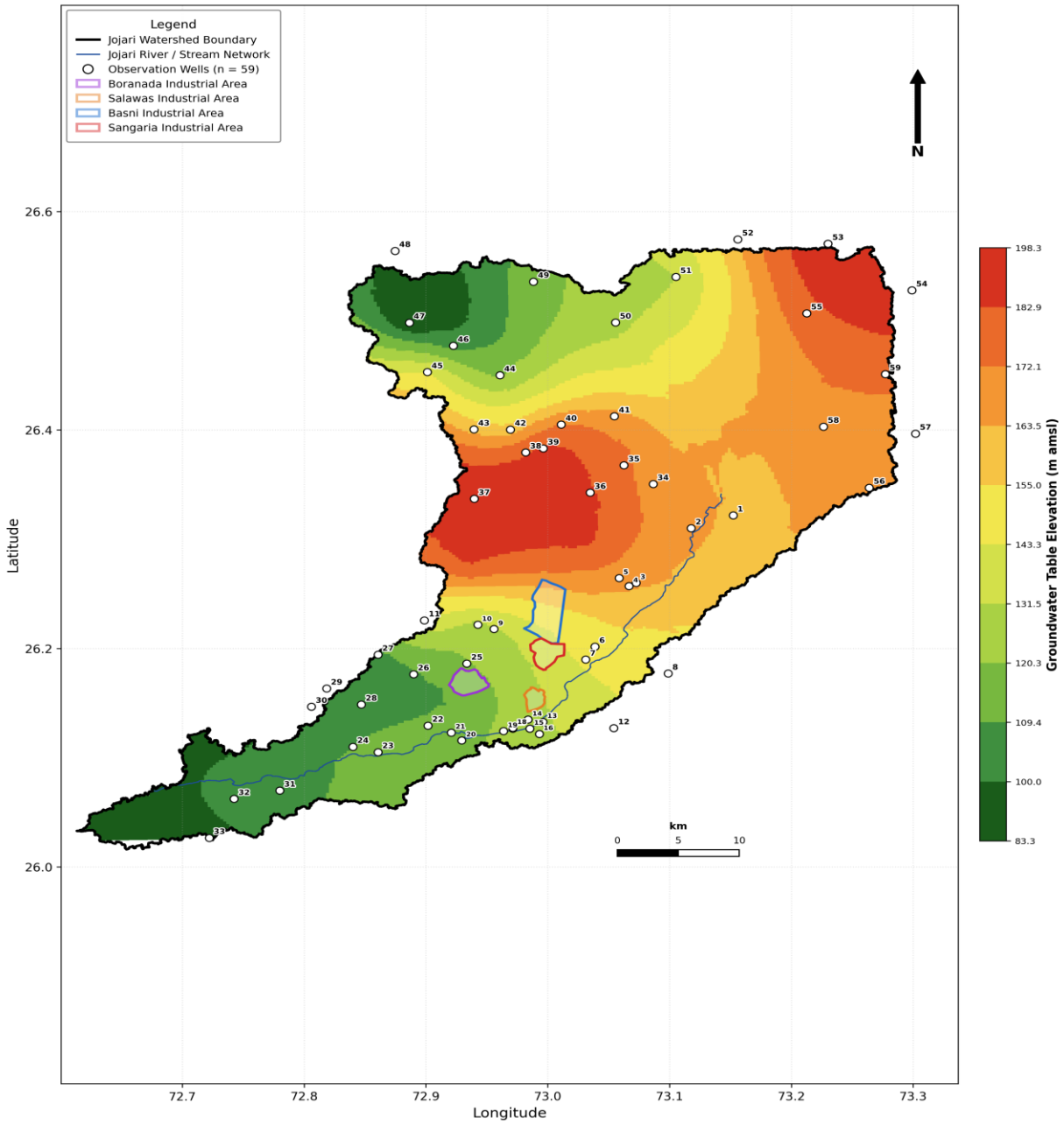


Fig. 4 Spatial distribution of groundwater table elevation (m above mean sea level) in the Jojari River watershed

4. Materials and Methods

4.1. Data Acquisition and Quality Control

The 59 records are secondary data: no samples were collected by the authors. They were taken from the routine pre-monsoon monitoring of GWD, CGWB and RSPCB for April-May 2025, including the National Aquifer Mapping (NAQUIM 2.0) studies for the Jodhpur urban agglomerate [34]. The agencies report that samples were analysed by the procedures of the APHA Standard Methods [35]; laboratory-level details such as instrument calibration and blanks were not available to the authors. The data set covers pH, Electrical Conductivity (EC), Total Dissolved Solids (TDS), the major cations (Ca^{2+}, Mg^{2+}, Na^{+} and K^{+}), the major anions (HCO_3^{-}, CO_3^{2-}, Cl^{-}, SO_4^{2-} and NO_3^{-}) and fluoride (F^{-}), with station codes and coordinates. Before analysis, the records were screened for completeness and internal consistency. The TDS/EC ratio ranges from 0.45 to 0.67 (median 0.60), reported total alkalinity agrees with the value calculated from HCO_3^{-} and CO_3^{2-} (median ratio 1.00), and reported total hardness agrees with the value calculated from Ca^{2+} and Mg^{2+} (median ratio 1.00). The Charge-Balance Error (CBE) was calculated from cation and anion sums in meq/L with Equation 1:

$$\text{CBE}\ (\%) = \frac{\sum\text{cations} - \sum\text{anions}}{\sum\text{cations} + \sum\text{anions}} \times 100 \qquad (1)$$

All 59 samples are within ±10% (median absolute CBE 0.8%, maximum 9.0%), and 40 of them (68%) are within ±5%. Although ±5% is the conventional target for laboratory analyses [36], the ±10% limit was retained for three reasons. (i) The records were compiled from routine monitoring by three agencies and several laboratories rather than from a single controlled campaign. (ii) Many samples are highly saline (EC up to 23,194 µS/cm and Cl^- up to 5,598 mg/L), and such samples require large dilutions before titration of Cl^- and flame photometry of Na^+ and K^+, which magnifies small analytical errors in the dominant ions. (iii) A charge balance alone does not establish analytical accuracy, because errors in different ions can offset one another [37]. A 10% limit has also been applied in a recent regional groundwater study in India [38]. To test whether this choice affects the results, the WQI classes, Piper facies and PCA structure were recomputed for the 40 samples within ±5% (Section 5.10).

4.2. Water Quality Index (WQI)

Drinking-water suitability was rated with a modified weighted arithmetic WQI. Eleven parameters (pH, EC, TDS, TH, Ca, Mg, Cl^-, SO_4^{2-}, NO_3^-, F^- and Na^+) were given unit weights (w_i) from 2 to 5 according to their importance for drinking water, with the highest weights for nitrate and fluoride because of their direct health effects. BIS IS 10500:2012 values [5] were used wherever a formal limit exists. EC (1,500 µS/cm) and Na^+ (200 mg/L) have no BIS limit; they were used as stated screening values and are not presented as BIS limits. The quality rating q_i for each parameter other than pH, the rating for pH, the relative weight W_i and the index were computed with Equations 2-5:

$$q_i = 100\left(\frac{C_i}{S_n}\right) \qquad (2)$$

$$q_{\text{pH}} = 100\left(\frac{V_{\text{pH}} - 7.0}{8.5 - 7.0}\right) \qquad (3)$$

$$W_i = \frac{w_i}{\sum_{i=1}^{n} w_i} \qquad (4)$$

$$\text{WQI} = \sum_{i=1}^{n} W_i\ q_i \qquad (5)$$

Where C_i is the measured concentration, S_n is the adopted standard or reference value, V_{pH} is the measured pH, 7.0 is the ideal pH, and 8.5 is the BIS upper acceptable limit for pH. EC and TDS are strongly correlated (r = 0.997), and keeping both gives the dissolved-salt load a combined weight of 0.206. They were kept because EC is the standard screening measure and TDS carries the BIS limit, and their effect was tested by recomputing the index without each of them (Section 5.10).

The unit weights follow the common practice of giving the highest weights to parameters with direct health effects (nitrate and fluoride) and to the main salinity measures; because any weighting scheme involves judgement, an equal-weight index was also computed. The WQI values were grouped into five classes: Excellent (< 50), Good (50-100), Poor (100-200), Very Poor (200-300) and Unsuitable for drinking (> 300). Table 1 lists w_i, S_n and W_i for each parameter.

Table 1. Unit weights, relative weights and adopted standard/reference values used for WQI calculation

Parameter	Unit weight (w_i)	Adopted standard/reference value (S_n)	Relative weight ($W_i = w_i/\Sigma w_i$)
pH	4	8.5 (deviation from 7.0)	0.1176
EC	3	1500 µS/cm*	0.0882
TDS	4	500 mg/L	0.1176
Total Hardness	2	600 mg/L	0.0588
Calcium	2	75 mg/L	0.0588
Magnesium	2	30 mg/L	0.0588
Chloride	3	250 mg/L	0.0882
Sulphate	3	200 mg/L	0.0882
Nitrate	5	45 mg/L	0.1471
Fluoride	4	1.0 mg/L	0.1176
Sodium	2	200 mg/L**	0.0588
Total	34	–	1.0000

** EC screening value adopted in this study (no BIS limit exists for EC). ** Sodium reference value based on the WHO taste threshold [39] (not a BIS limit). Other S_n values are BIS IS 10500:2012 acceptable limits, except total hardness, for which the permissible limit is used (Section 4.2). W_i values are rounded to four decimals.*

The values of S_n in Table 1 differ from some of the limits in Table 2, and the reason is explained here. For calcium, the WQI uses the BIS acceptable (desirable) limit of 75 mg/L, while Table 2 reports the permissible limit of 200 mg/L. The same applies to magnesium (30 and 100 mg/L), TDS (500 and 2,000 mg/L), chloride (250 and 1,000 mg/L), sulphate (200 and 400 mg/L) and fluoride (1.0 and 1.5 mg/L). The WQI measures how far a sample departs from good drinking quality, so the acceptable limit is the appropriate reference: a rating of $q_i = 100$ means that the acceptable limit has been reached. The permissible limit applies only when no alternative source is available, and it is therefore used in Table 2 to show how many wells fail even the relaxed standard. Total hardness is the one exception. Its permissible limit (600 mg/L as $CaCO_3$) was used as S_n because hardness has no health-based guideline value, and the acceptable limit of 200 mg/L would inflate the index through a largely aesthetic parameter in this naturally hard-water terrain.

4.3. Irrigation Water Quality Indices

Irrigation suitability was assessed with three indices computed from ion concentrations in meq/L (Equations 6-8):

$$\mathrm{SAR} = \frac{\mathrm{Na^+}}{\sqrt{(\mathrm{Ca^{2+}}+\mathrm{Mg^{2+}})/2}} \quad (6)$$

$$\%\mathrm{Na} = \frac{\mathrm{Na^+}+\mathrm{K^+}}{\mathrm{Ca^{2+}}+\mathrm{Mg^{2+}}+\mathrm{Na^+}+\mathrm{K^+}} \times 100 \quad (7)$$

$$\mathrm{RSC} = (\mathrm{CO_3^{2-}} + \mathrm{HCO_3^-}) - (\mathrm{Ca^{2+}} + \mathrm{Mg^{2+}}) \quad (8)$$

Salinity and sodium hazard were also classified on the USSL diagram of Richards [40], which plots SAR against EC and assigns each sample to one of sixteen classes (C1-C 4 for salinity and S1-S4 for sodium). The percent-sodium classes follow Wilcox [41].

4.4. Hydrochemical Facies and Geochemical Controls

The facies of each sample was determined from its major-ion percentages (meq/L) on a Piper diagram [6], which classifies water by its dominant cation (Ca^{2+}, Mg^{2+} or $Na^+ + K^+$) and anion ($HCO_3^- + CO_3^{2-}$, SO_4^{2-} or Cl^-). To identify the broad natural controls (rock–water interaction, evaporation and crystallisation, or rainfall), samples were plotted on Gibbs diagrams [7] of TDS against $Na^+/(Na^+ + Ca^{2+})$ and $Cl^-/(Cl^- + HCO_3^-)$.

4.5. Multivariate Statistical Analysis

Pearson correlation coefficients were computed among all parameters. PCA was run on the standardised (z-score) matrix of pH, EC, TDS, TH, Ca^{2+}, Mg^{2+}, Na^+, K^+, Cl^-, SO_4^{2-}, HCO_3^-, NO_3^- and F^-, following the approach of comparable regional studies [11, 13, 19, 27]. The number of components was judged by the Kaiser criterion (eigenvalue > 1) and by Horn's parallel analysis with 1,000 random data sets [42]. Component stability was assessed with Tucker's congruence coefficient [43] between the full solution and solutions from (i) 1,000 bootstrap resamples, (ii) log-transformed data, (iii) the data set without the four extreme wells of Cluster 2, (iv) the 40 samples within ±5% CBE and (v) a data set without TDS. HCA with Ward's minimum-variance linkage on the same matrix grouped the 59 wells into clusters, which were then compared with block and WQI class. The number of clusters was examined with the dendrogram linkage heights and the mean silhouette width [44], and cluster stability was assessed by the bootstrap Jaccard coefficient [45] and by the Adjusted Rand Index (ARI) between Ward's partition and those from k-means, average and complete linkage, and log-transformed data.

4.6. Spatial Interpolation and GIS Mapping

Maps of EC, TDS, Cl^-, SO_4^{2-}, Na^+, NO_3^- and F^- were prepared in ArcGIS/ArcMap by IDW interpolation [18], with a power of 2 and a variable search radius using the 12 nearest wells. All layers were projected to WGS 1984 UTM Zone 43N. The surfaces were clipped to the watershed boundary and overlaid with the river network, industrial-area boundaries and wells. The same coordinate system, interpolation settings, class scheme and layout were used for all maps. Mapping accuracy was evaluated by leave-one-out cross-validation: each well was removed in turn, its value was predicted from the remaining wells with the same settings, and the Mean Error (ME), Root-Mean-Square Error (RMSE) and observed–predicted correlation were computed; powers of 1 and 3 were also tested. The geological map (Figure 3) was prepared from a principal-aquifer shapefile with three units (granite and acidic crystalline rocks, sandstone with shale, and shale with sandstone). The water-table map (Figure 4) was prepared from a static water-level elevation raster based on pre-monsoon 2025 Groundwater Level (GWL) data, using the same cartographic framework.

IDW was chosen over kriging for three reasons. First, kriging depends on a reliable semi variogram, and about 100 to 150 points are generally needed to estimate one with confidence [46]; the present 59 wells, spread unevenly over the watershed and densest in Luni block, are below that range. Second, the main variables are strongly skewed (EC from 530 to 23,194 µS/cm), and even after a log transformation, the few extreme wells near the industrial areas would strongly influence a variogram fitted to so small a data set. Third, comparative studies have found that IDW often performs as well as kriging and that the better method depends on sample density and data variability [29, 30]. IDW is exact at the wells and makes no assumption about stationarity, but it can produce "bullseye" rings around isolated high values, and such rings appear around a few wells in Figures 5-11. For this reason, the maps are used only to show regional patterns. All quantitative conclusions rest on the measured well values and on the proximity statistics described below, not on interpolated values.

To test the influence of the industrial corridor directly, the straight-line (Euclidean) distance from each well to the boundary of the nearest of the four industrial-area polygons was computed in UTM coordinates with Python. Each well was assigned its nearest industrial area and distance. This distance was tested against every parameter with Pearson correlation and simple linear regression, and wells within and beyond 3 km of the nearest boundary were compared with the Mann-Whitney U test; the comparison was repeated at 2 km and 5 km. Significance was judged at $p < 0.05$. Because the salinity indicators are strongly intercorrelated, they were interpreted as one group rather than as independent tests. Five sensitivity tests were then applied: (i) Spearman rank correlation, which limits the influence of extreme values; (ii) repetition without the four extreme wells of Cluster 2; (iii) leave-one-out recalculation of r; (iv) partial correlation controlling for UTM easting and northing, which represent the regional south-westward gradient in water-table elevation and salinity; and (v) a within-block test restricted to Luni block (n = 28). As hydrogeological evidence, the near-corridor wells were also classified as down-gradient or up- and cross-gradient of the nearest industrial area, using the regional flow direction inferred from Figure 4. Straight-line distance ignores aquifer heterogeneity and the actual flow path, so the test remains a correlational screening tool rather than a transport model.

4.7. Integration of Methods

The methods were combined in a fixed sequence so that each step constrains the next. (i) Data screening (charge balance and internal consistency) defines the usable data set. (ii) The WQI and irrigation indices describe suitability but say nothing about sources. (iii) Piper and Gibbs diagrams identify the natural processes that set the background chemistry, here evaporation and rock–water interaction. (iv) Correlation, PCA and HCA separate groups of co-varying parameters and wells, which are candidate source signals. (v) The proximity analysis then tests each candidate signal against an expected spatial behaviour.

An industrial saline effluent should raise Na^+, Cl^-, SO_4^{2-} and TDS near the industrial boundaries without raising nitrate; a geogenic fluoride source should follow alkalinity and lithology and show no distance relationship; and a diffuse sewage or agricultural source should raise nitrate independently of industrial distance.

(vi) Sensitivity analyses check whether each conclusion holds under alternative data screening, index formulation, statistical choices and controls for regional trends. A source is regarded as supported only when the chemical signature, the multivariate grouping and the spatial test agree, and as probable but unconfirmed when the spatial test is not robust.

5. Results and Discussion

5.1. General Hydrochemistry

Table 2 gives descriptive statistics for the 15 parameters, the BIS limits and reference values, and the share of samples above each. The groundwater is alkaline, with pH from 7.30 to 9.20 (mean 8.14); 13.6% of samples lie outside the BIS range of 6.5–8.5. EC varies widely, from 530 to 23,194 µS/cm (mean 5,418 µS/cm), and 86.4% of wells exceed the screening value of 1,500 µS/cm (not a BIS limit), which points to salinization across the watershed. TDS follows EC closely (r = 0.997), ranging from 242 to 15,540 mg/L (mean 3,381 mg/L); 61.0% of samples exceed the permissible limit of 2,000 mg/L and 95% exceed the acceptable limit of 500 mg/L.

Table 2. Descriptive statistics of groundwater physicochemical parameters and BIS/reference limits (n = 59, pre-monsoon 2025)

Parameter	Min	Max	Mean	SD	BIS limit	% exceeding
pH	7.30	9.20	8.14	0.44	6.5–8.5	13.6
EC (µS/cm)	530.0	23,194.0	5,418.2	4,372.0	1500*	86.4
TDS (mg/L)	241.9	15,540.0	3,380.5	2,894.5	2000 (P)	61.0
Carbonate (mg/L)	1.4	396.1	46.5	66.9	–	–
Bicarbonate (mg/L)	12.0	1,000.7	312.0	193.7	–	–
Total Alkalinity (mg/L)	39.1	1,480.4	319.0	244.9	–	–
Chloride (mg/L)	35.5	5,598.0	1,263.6	1,131.6	1000 (P)	47.5
Nitrate (mg/L)	5.4	463.8	98.7	119.5	45	55.9
Sulphate (mg/L)	19.2	2,217.0	320.2	407.0	400 (P)	20.3
Fluoride (mg/L)	0.08	12.65	2.72	2.84	1.5 (P)	54.2
Total Hardness (mg/L)	170.0	1,540.0	552.6	303.8	600 (P)	32.2
Calcium (mg/L)	24.0	336.0	105.9	71.0	200 (P)	13.6
Magnesium (mg/L)	15.8	237.1	70.0	41.7	100 (P)	20.3
Sodium (mg/L)	37.3	3,405.2	832.4	678.4	200**	89.8
Potassium (mg/L)	1.2	114.2	24.6	24.6	–	–

*(P) BIS IS 10500:2012 permissible limit in the absence of an alternate source; pH and nitrate limits have no relaxation. * EC screening value adopted in this study (not a BIS limit). ** Sodium reference value based on the WHO taste threshold [39] (not a BIS limit). The WQI uses the acceptable limits listed in Table 1.*

Chloride (35–5,598 mg/L, mean 1,264 mg/L) and sodium (37–3,405 mg/L, mean 832 mg/L) are the most enriched ions. Chloride exceeds the permissible limit of 1,000 mg/L in 47.5% of samples, and sodium exceeds the reference value of 200 mg/L in 89.8%. Sulphate (19–2,217 mg/L, mean 320 mg/L) exceeds 400 mg/L in 20.3% of samples. Nitrate ranges from 5.4 to 464 mg/L (mean 99 mg/L) and exceeds the BIS limit of 45 mg/L in 55.9% of wells.

This pattern suggests loading from sewage and fertilizer rather than from the salinity process, as reported elsewhere in semi-arid Rajasthan [2, 21] (Section 5.7). Fluoride ranges from 0.08 to 12.65 mg/L (mean 2.72 mg/L); 54.2% of samples exceed the permissible limit of 1.5 mg/L and 66% exceed the acceptable limit of 1.0 mg/L. Fluoride is therefore a widespread health concern when judged against both BIS and WHO [39] values, which fits the fluoride-prone crystalline geology of the Marwar region and results from other semi-arid and hard-rock parts of India [16, 19].

5.2. Spatial Distribution of Key Parameters

The IDW maps (Figures 5-11) show high EC, TDS, chloride and sodium, and to a lesser degree sulphate and fluoride, in the downstream south-western part of the watershed, mostly in Luni block, with a second zone of high values near the Basni, Sangaria, Salawas and Boranada industrial belt. Two processes are likely responsible: evaporative concentration of groundwater as it moves downstream in a high-evapotranspiration setting, and the added load from industrial and urban effluent seepage in the lower watershed; the second is tested directly in Section 5.9. Nitrate (Figure 10) follows a different pattern: it is not concentrated near the industrial belt but shows local peaks in the outer cropland areas of the watershed, consistent with fertilizer and irrigation return flow. Mandore and Tinwari blocks, in the upper and outer parts of the watershed, generally show lower values, though many wells there still exceed BIS limits. Some isolated high-value rings on the maps are IDW artefacts around single wells (Section 4.6) and should not be read as separate plumes.

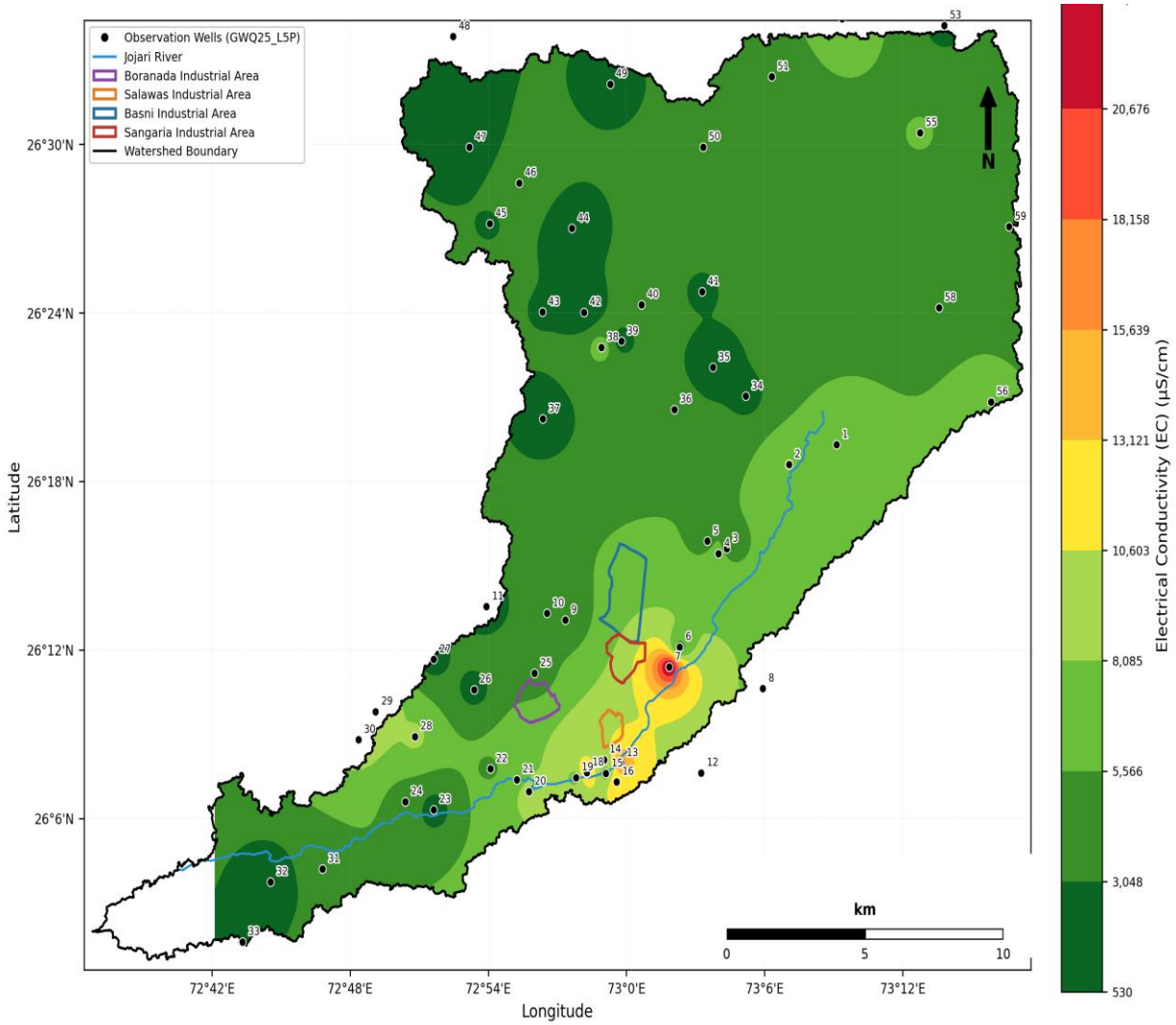


Fig. 5 Spatial distribution of electrical conductivity (EC, µS/cm) in groundwater, Jojari watershed, pre-monsoon 2025

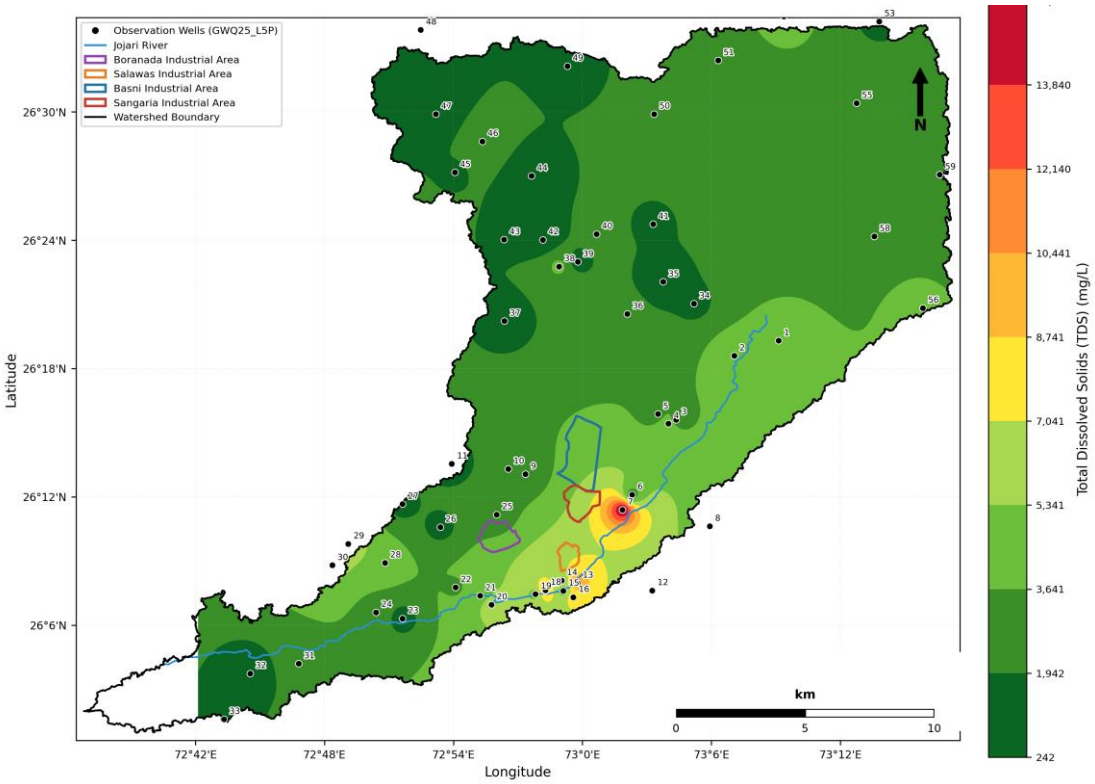


Fig. 6 Spatial distribution of total dissolved solids (TDS, mg/L) in groundwater, Jojari watershed, pre-monsoon 2025

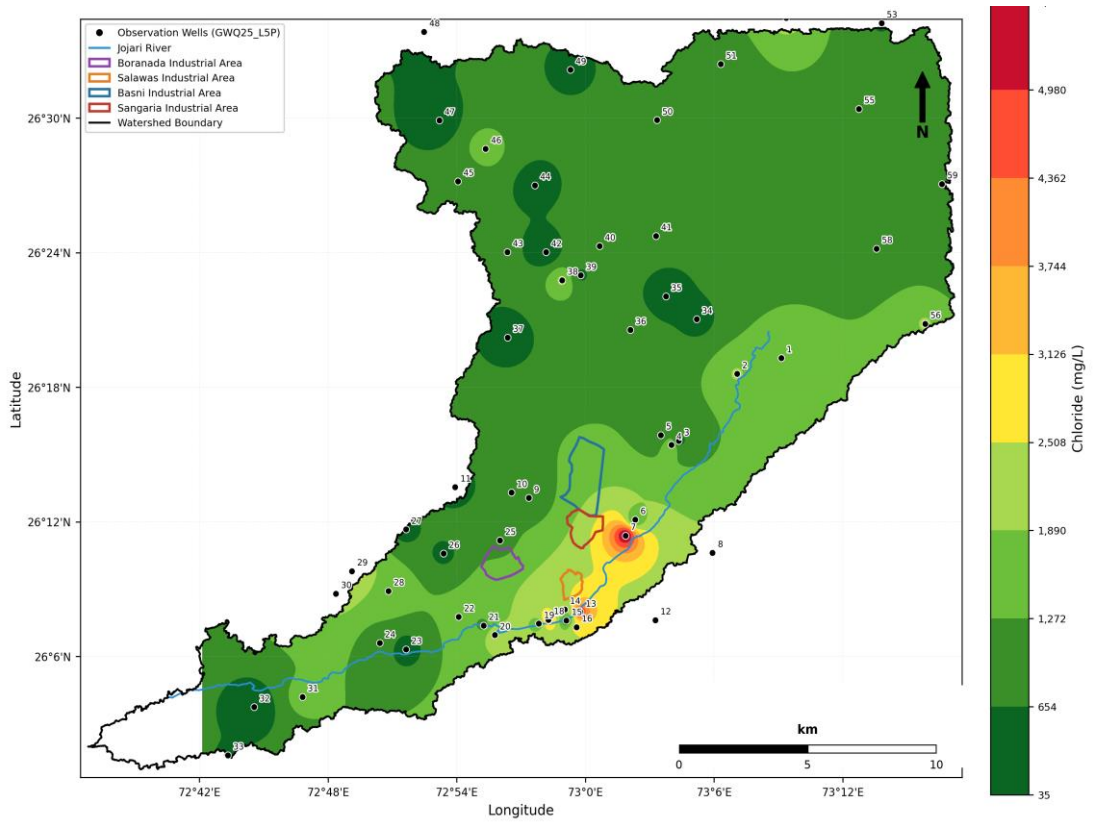


Fig. 7 Spatial distribution of chloride (Cl^-, mg/L) in groundwater, Jojari watershed, pre-monsoon 2025

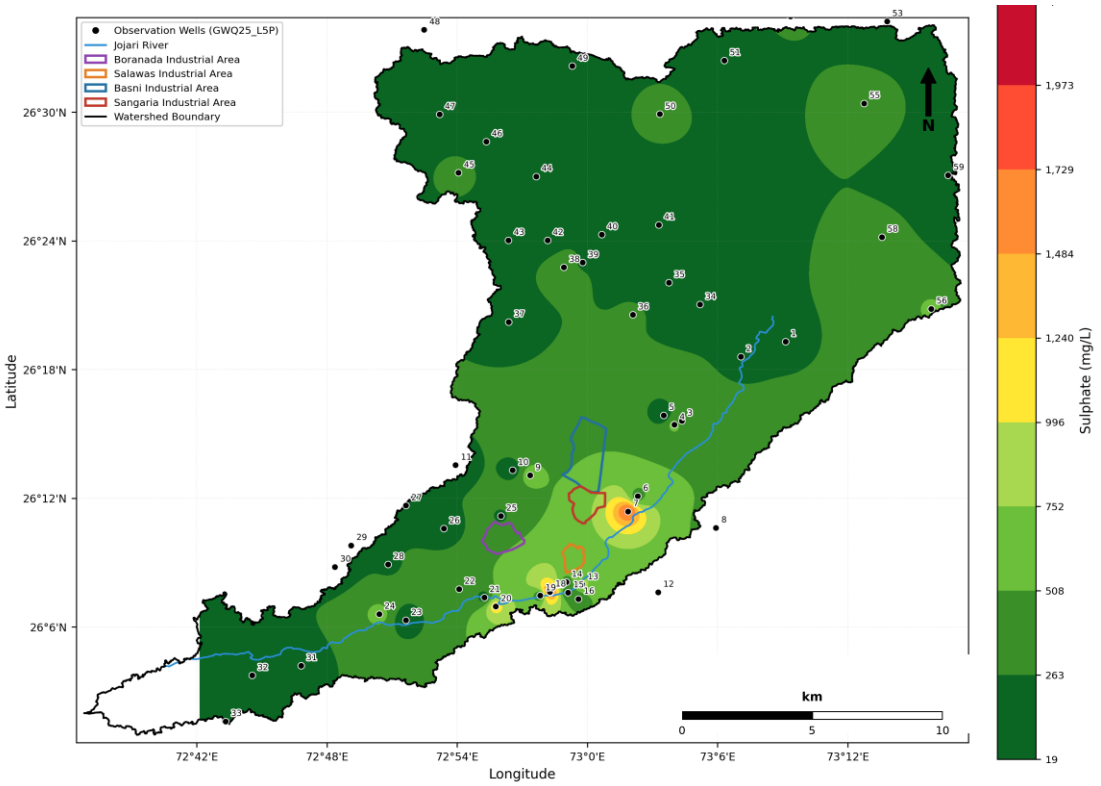


Fig. 8 Spatial distribution of Sulphate (SO_4^{2-}, mg/L) in groundwater, Jojari watershed, pre-monsoon 2025

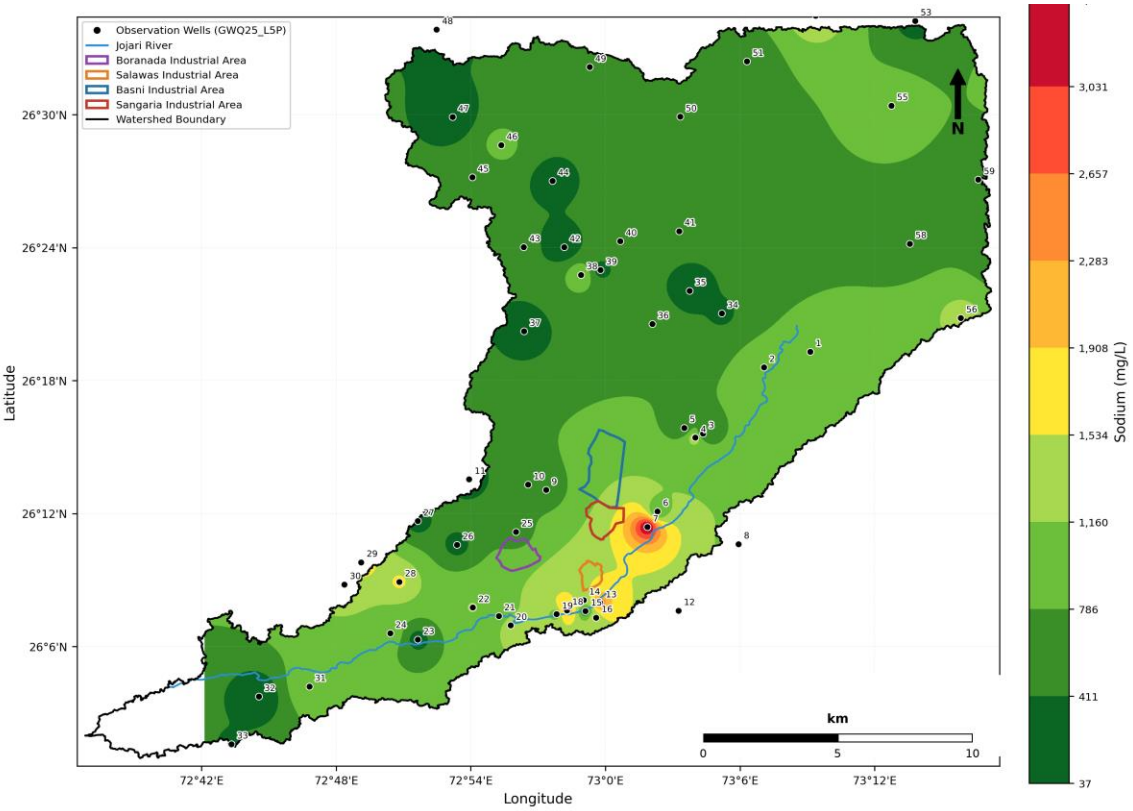


Fig. 9 Spatial distribution of Sodium (Na^+, mg/L) in groundwater, Jojari watershed, pre-monsoon 2025

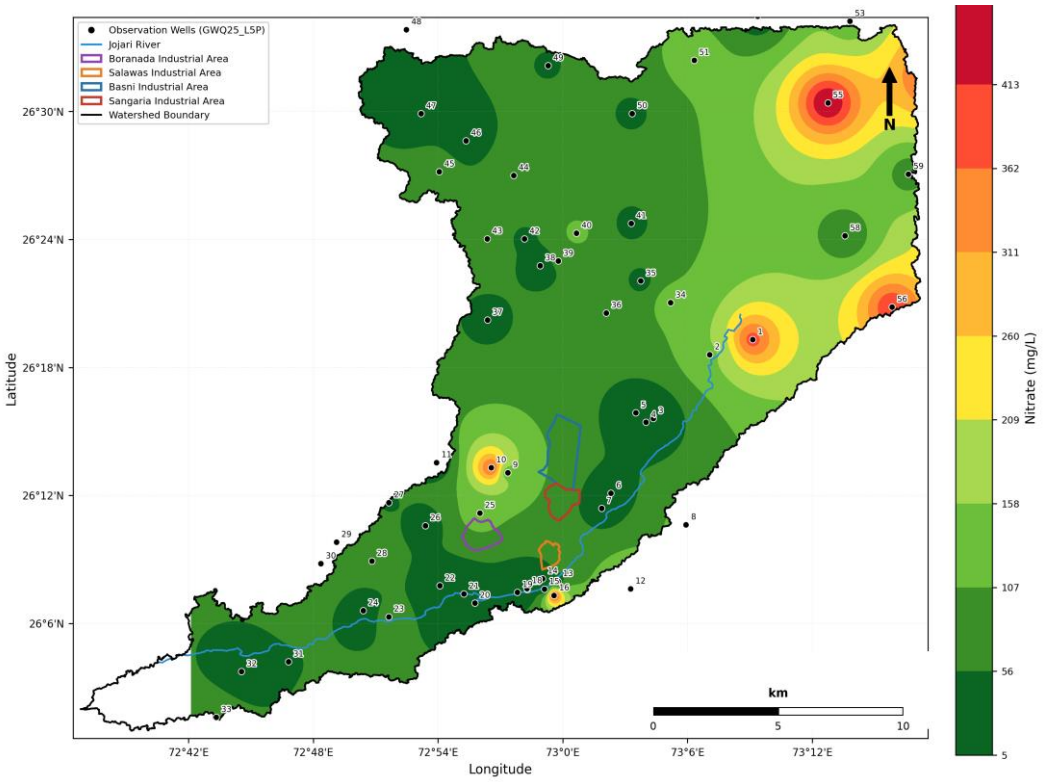


Fig. 10 Spatial distribution of Nitrate (NO_3^-, mg/L) in groundwater, Jojari watershed, pre-monsoon 2025

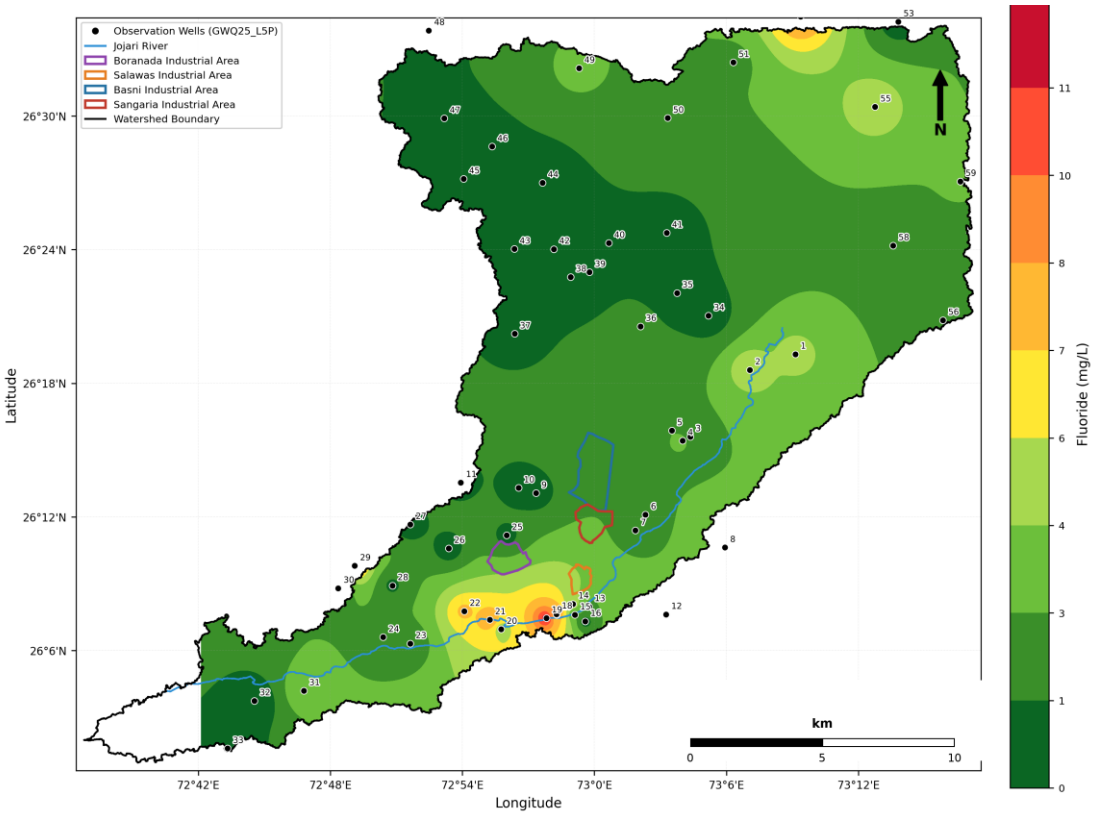


Fig. 11 Spatial distribution of Fluoride (F^-, mg/L) in groundwater, Jojari watershed, pre-monsoon 2025

5.3. Water Quality Index and Drinking-Water Suitability

WQI values vary widely across the 59 wells. Only 3.4% of samples are Excellent and 8.5% Good; the other 88.1% are Poor (27.1%), Very Poor (22.0%) or Unsuitable for drinking (39.0%) (Table 3, Figure 12). Mean WQI is highest in Luni block (366.1, range 38.7–951.6, n = 28), followed by Baori (318.8, n = 6), Mandore (222.9, n = 21) and Tinwari (144.6, n = 4) (Figure 13); the Baori and Tinwari means rest on few wells and should be read with caution. Luni, the most downstream block in the watershed and the one most exposed to both salinity and effluent pressure, is thus the main quality hotspot. Other WQI studies in Rajasthan and the wider semi-arid belt of India have also found large shares of wells unfit for drinking without treatment [11, 16, 20].

Table 3. Classification of groundwater samples by WQI, Jojari watershed, pre-monsoon 2025 (n = 59)

WQI class	Range	No. of wells	% of wells
Excellent	< 50	2	3.4
Good	50–100	5	8.5
Poor	100–200	16	27.1
Very Poor	200–300	13	22.0
Unsuitable for drinking	> 300	23	39.0

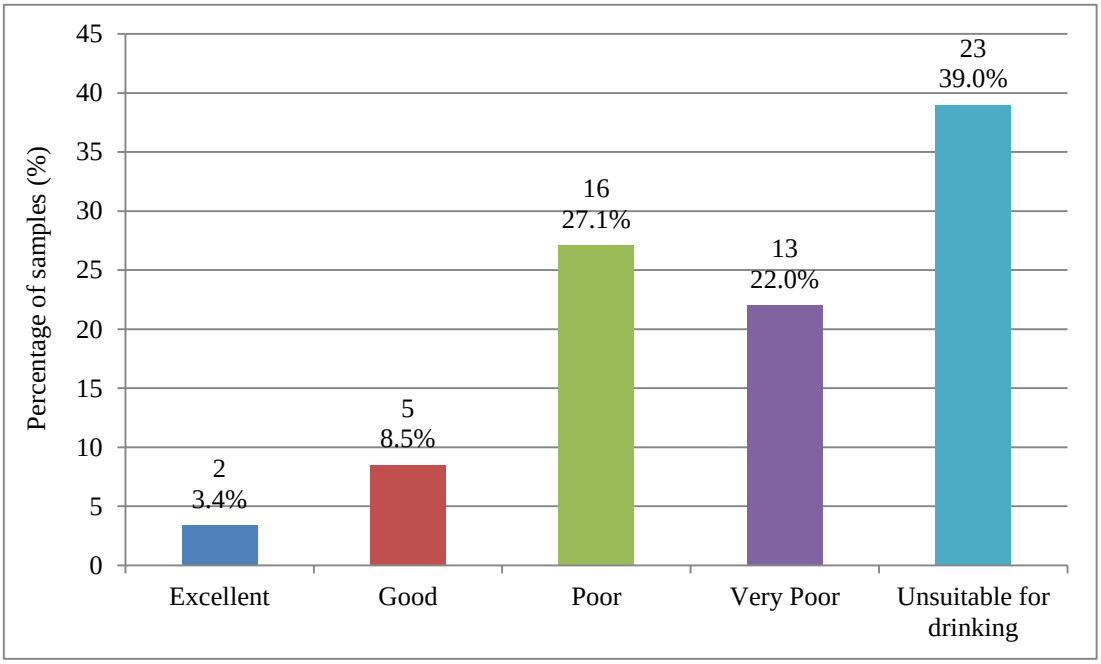


Fig. 12 Classification of groundwater samples by Water Quality Index (WQI) category

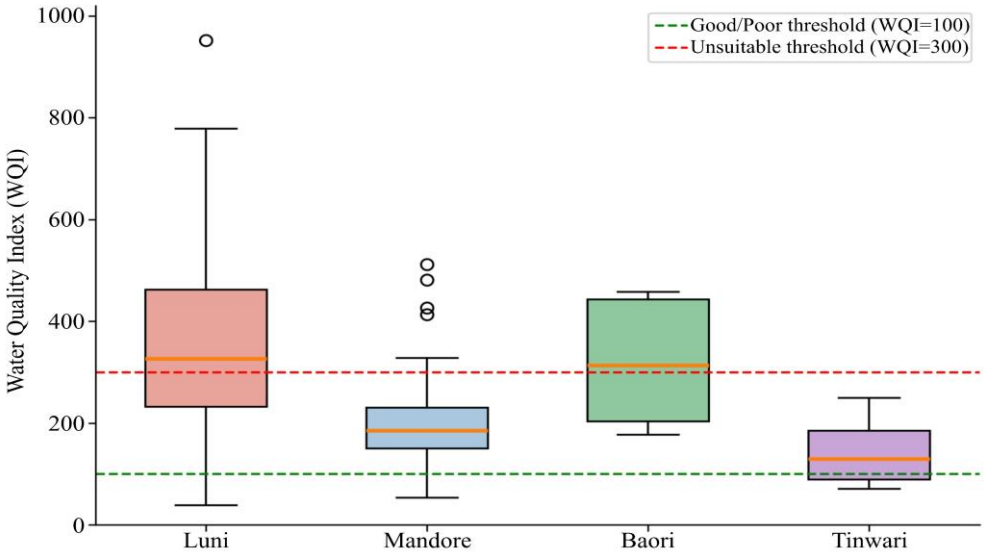


Fig. 13 Block-wise distribution of WQI values across the four administrative blocks of the Jojari watershed

5.4. Hydrochemical Facies

On the Piper diagram **(**Figure 14), about 85% of samples (50 of 59) fall in the Na + K-Cl field, and only a few are mixed or bicarbonate types. Such strong Na-Cl dominance points to evaporative concentration in an arid, semi-closed drainage, helped by rock–water interaction, dissolution of soluble salts and possibly cation exchange and, at the sites nearest the industrial areas, probably by seepage of saline wastewater (Section 5.9). Ca-HCO_3 water, which usually marks fresh and recently recharged groundwater, is almost absent. Very little of the sampled groundwater therefore carries the signature of recent recharge, as expected from the low and erratic rainfall.

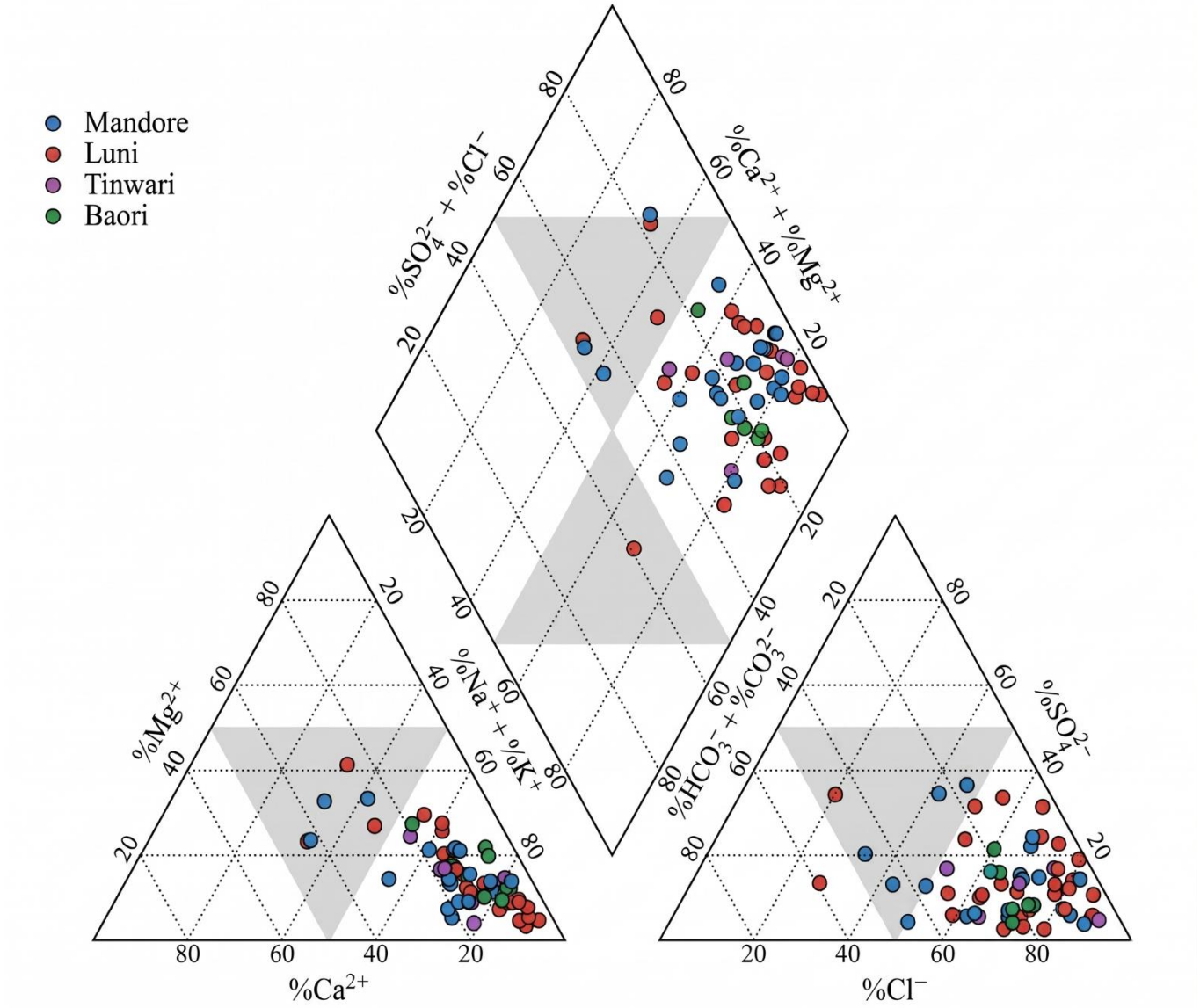


Fig. 14 Piper trilinear diagram of hydrochemical facies for the groundwater samples (n = 59), colour-coded by administrative block, Jojari watershed, pre-monsoon 2025

5.5. Geochemical Controls on Water Chemistry

The Gibbs diagrams (Figure 15) plot TDS against $Na^+/(Na^+ + Ca^{2+})$ and $Cl^-/(Cl^- + HCO_3^-)$ and separate rainfall, rock–water interaction and evaporation as controls on natural water chemistry. Most samples fall in the evaporation field and move towards the evaporation-crystallization end-member (labelled "Seawater" in the original Gibbs scheme) at high TDS and high ionic ratios, a few lower-TDS samples lie in the rock-dominance field, and none plot in the rainfall field. Evaporative concentration and rock-water interaction, not dilution by fresh recharge, therefore control groundwater chemistry across the watershed. Because the Gibbs scheme was developed for natural waters, it cannot separate evaporative salinity from salt added by effluent; that distinction is tested in Section 5.9. Similar evaporation-dominated behaviour has been reported for semi-arid hard-rock aquifers in southern India [19], whereas chemical weathering dominates in a less arid part of Rajasthan [1].

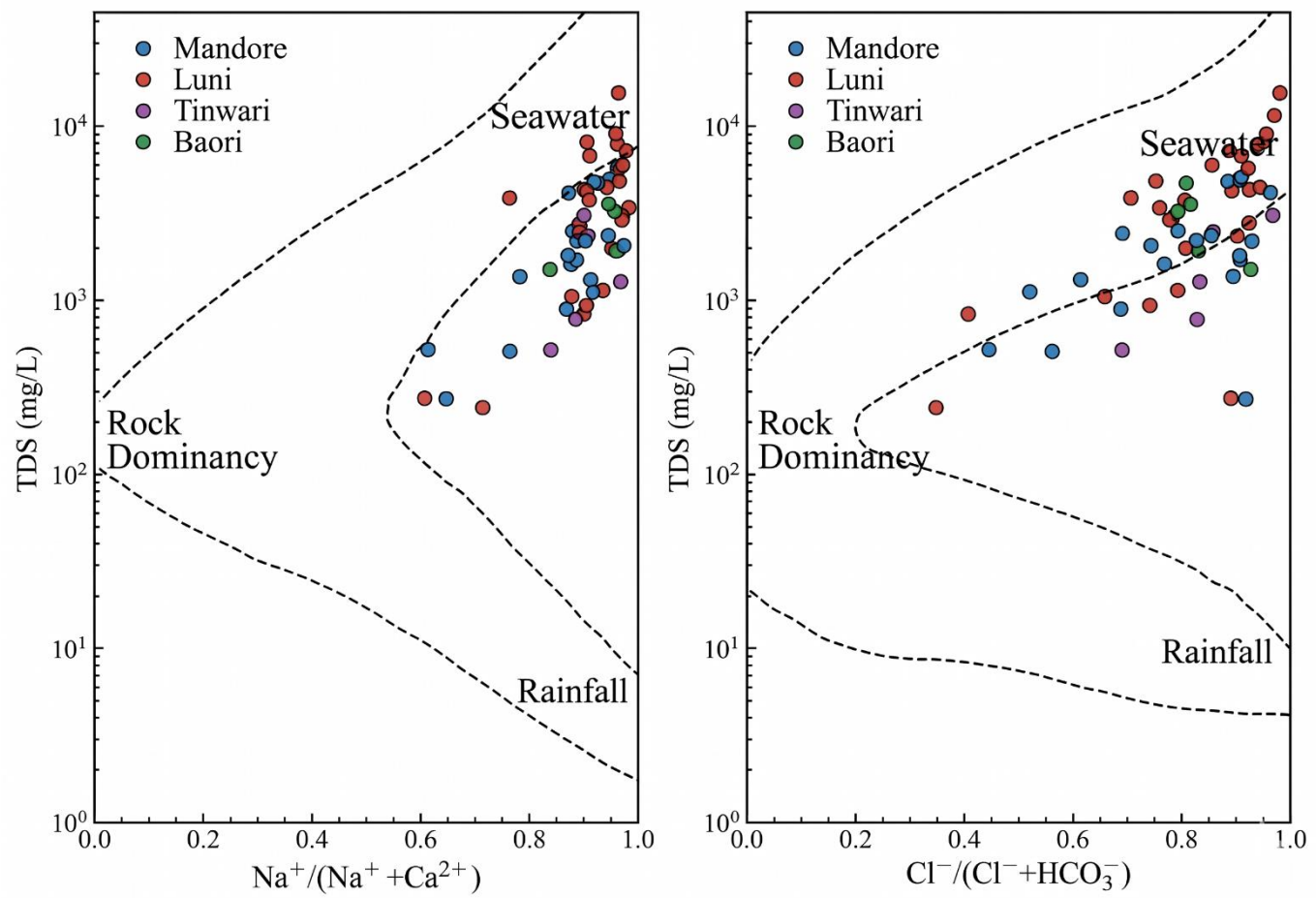


Fig. 15 Gibbs diagrams: (a) TDS vs. $Na^+/(Na^+ + Ca^{2+})$; (b) TDS vs. $Cl^-/(Cl^- + HCO_3^-)$, showing evaporation dominance as the principal control on groundwater chemistry

5.6. Irrigation Water Quality

Table 4 gives the irrigation classes. By SAR, 37.3% of samples are Excellent (< 10) and 30.5% Good (10–18), but 32.2% are Doubtful (18–26) or Unsuitable (> 26), a significant sodium hazard concentrated in the more saline parts of Luni and Baori blocks. Percent sodium is stricter: 83.1% of samples are Doubtful (60–80%) or Unsuitable (> 80%), in line with the Na dominance seen on the Piper diagram. The difference arises because %Na reflects only the proportion of sodium among the cations, whereas SAR also accounts for the absolute Ca and Mg concentrations, which are high in this hard groundwater (mean total hardness 553 mg/L as $CaCO_3$) and partly offset the sodium effect. RSC, in contrast, places 83.1% of samples in the Good class (< 1.25 meq/L) and only 13.6% in the Unsuitable class (> 2.5 meq/L).

RSC depends on the balance between carbonate alkalinity and Ca + Mg rather than on total salinity, and because most Jojari groundwater is chloride-dominated rather than bicarbonate-dominated, it carries little carbonate hazard even where salinity is high; the few wells with RSC above 2.5 meq/L are the exception.

Table 4. Classification of groundwater samples for irrigation by SAR, %Na and RSC, Jojari watershed, pre-monsoon 2025 (n = 59)

Index	Class	% of wells
SAR	Excellent (< 10)	37.3
	Good (10–18)	30.5
	Doubtful (18–26)	18.6
	Unsuitable (> 26)	13.6
%Na	Excellent (< 20)	0.0
	Good (20–40)	6.8
	Permissible (40–60)	10.2
	Doubtful (60–80)	55.9
	Unsuitable (> 80)	27.1
RSC	Good (< 1.25)	83.1
	Doubtful (1.25–2.5)	3.4
	Unsuitable (> 2.5)	13.6

On the USSL diagram (Figure 16**)**, most samples fall in the high to very high salinity classes (C3- C4) and spread across all sodium classes (S1–S4). Several Luni-block wells plot in C4-S3 and C4-S4, and the seven wells with EC above 10,000 µS/cm, which lie beyond the diagram, also fall in class

C4. In these zones, safe long-term use needs leaching and salt-tolerant crops to manage salinity, and gypsum to counter the sodium hazard. Carbonate hazard is limited, but the high salinity hazard makes much of the groundwater marginal or unsuitable for salt-sensitive crops unless it is treated or blended.

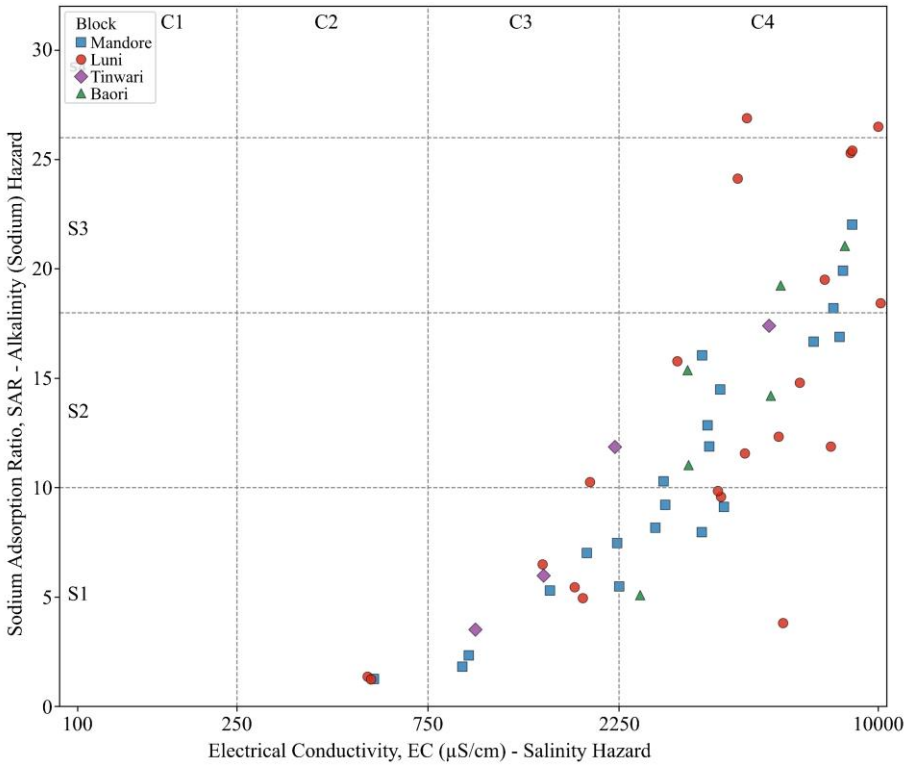


Fig. 16 USSL diagram (after Richards, 1954) classifying groundwater samples by salinity hazard (C1-C4) and sodium hazard (S1–S4), colour-coded by administrative block; wells with EC above 10,000 µS/cm (n = 7) plot beyond the diagram and fall in class C4

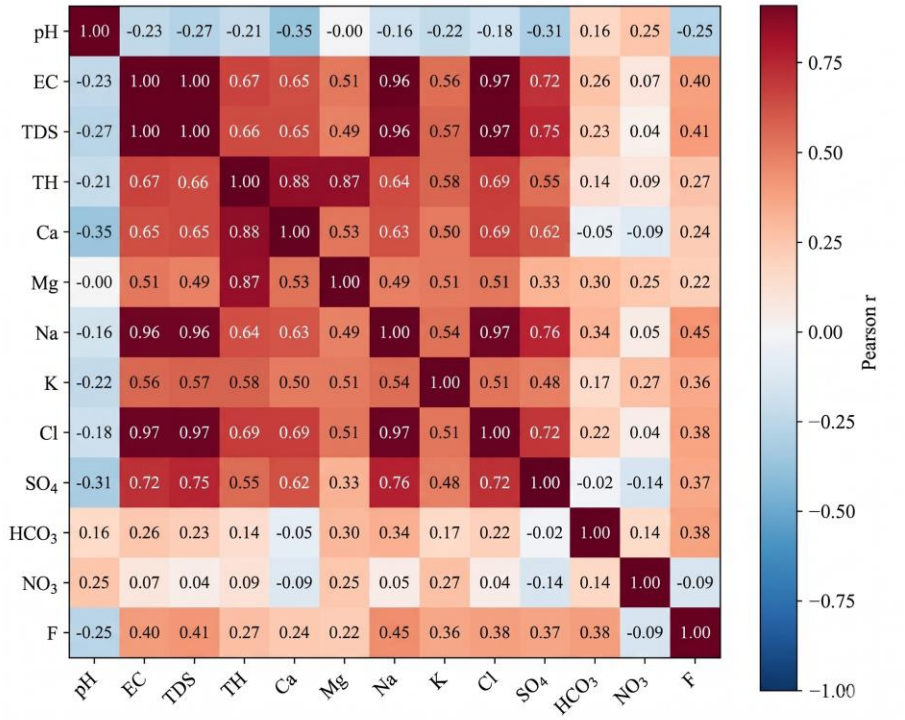


Fig. 17 Pearson correlation matrix of groundwater quality parameters, Jojari watershed, pre-monsoon 2025 (n = 59)

5.7. Multivariate Statistical Analysis

5.7.1. Correlation Analysis

The Pearson matrix (Figure 17) shows very strong positive correlations among EC, TDS, Cl^- and Na^+ (r = 0.96–0.997), a single salinity group with shared controls on the bulk ionic load. With n = 59, correlations with |r| > 0.26 are significant at $p < 0.05$. Sulphate correlates moderately with EC (r = 0.72), and Ca^{2+} and Mg^{2+} correlate only moderately with each other (r = 0.53), which suggests partly separate sources such as carbonate, silicate or gypsum dissolution. Nitrate correlates weakly with pH (r = 0.25), fluoride (r = −0.09) and bicarbonate (r = 0.14) and is not linked to the EC-TDS-Cl-Na group (r = 0.04–0.07). This suggests that nitrate is controlled by a separate process, most likely farm return flow or domestic sewage.

5.7.2. Principal Component Analysis

PCA on the 13 standardized parameters was run in IBM SPSS Statistics with principal component extraction and Varimax rotation with Kaiser normalization. The Kaiser–Meyer–Olkin measure was 0.692, above the acceptable threshold of 0.6, and Bartlett's test of sphericity was highly significant ($\chi^2 = 1324.9$, df = 78, $p < 0.001$), so the data are suitable for factor extraction. Three components had eigenvalues above 1 (6.78, 1.65 and 1.29) and, after rotation, together explain 74.7% of the total variance (PC1 = 45.08%, PC2 = 16.55%, PC3 = 13.06%) (Figure 18, Table 5). Parallel analysis is stricter: only PC1 exceeds the 95th percentile of random eigenvalues (2.10), while PC2 and PC3 fall just below theirs (1.79 and 1.58). PC2 and PC3 were nevertheless retained because they are chemically coherent and reappear in every sensitivity data set (Section 5.10), but they are interpreted with more caution than PC1.

After rotation, PC1 loads on TH, Ca, Cl, EC, TDS, Na, Mg, SO_4^{2-} and K (0.69–0.93). It is a salinization and mineralisation factor that reflects evaporative concentration and mineral dissolution (Section 5.5). PC2 loads on bicarbonate (0.76) and fluoride (0.70), with moderate loadings on Cl, EC, TDS and Na (0.44-0.56). It is an alkalinity-linked geogenic fluoride factor: in bicarbonate-rich water, calcite precipitation removes Ca^{2+} and allows further fluorite dissolution, and at high pH, OH^- can replace F^- on clay surfaces. PC3 loads on nitrate (0.75) and pH (0.65), with moderate loadings on sulphate (−0.42), bicarbonate (0.42) and Mg (0.40). It is a nitrate factor, most likely of human origin, separate from PC1 and from the industrial salinity gradient (Section 5.9); the positive pH loading may reflect alkaline sewage or wastewater inputs. In the unrotated solution, the first component alone explained 52.1% of the variance but mixed the salinity and fluoride signals; rotation separates them into three chemically meaningful factors.

Because EC and TDS are almost collinear (r = 0.997), the PCA was repeated without TDS. The rotated first component kept the same salinity structure (TH 0.93, Ca 0.87, Cl 0.83, EC 0.82, Na 0.79, Mg 0.76, SO_4^{2-} 0.70, K 0.69) and explained 44.3% of the variance. The PC1 interpretation is therefore not an artefact of the redundant TDS variable.

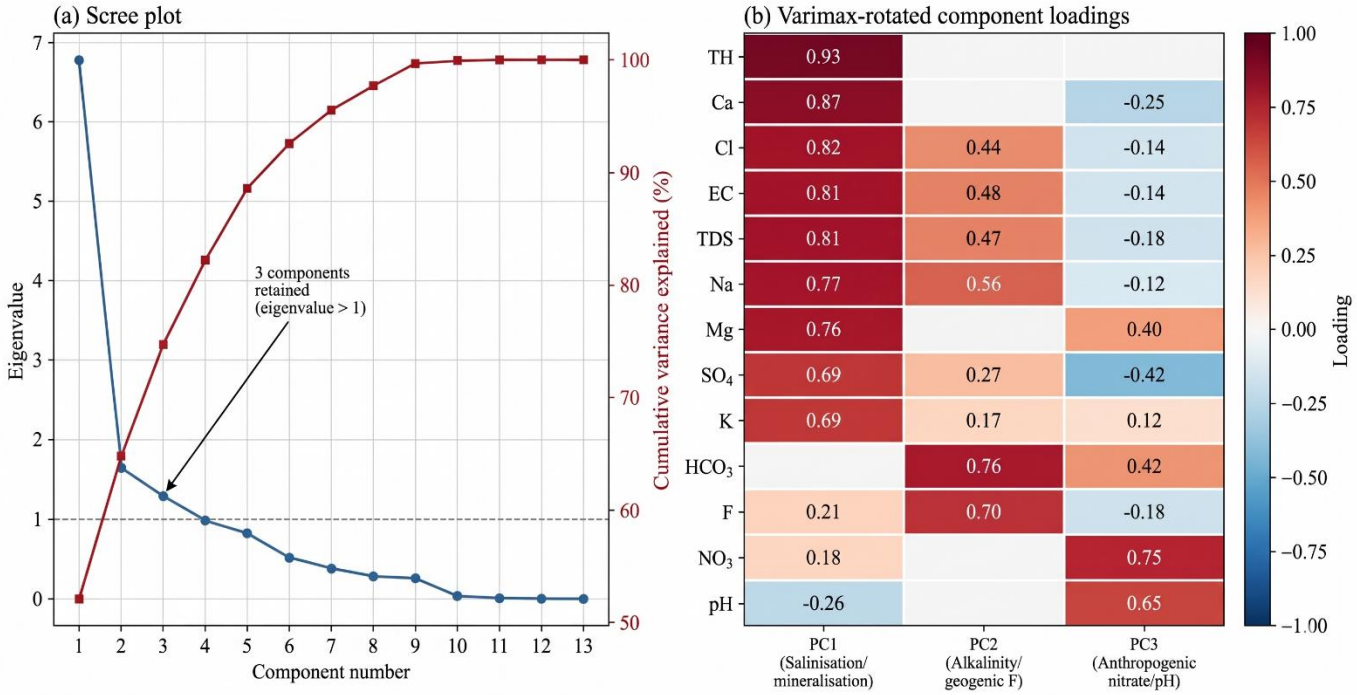


Fig. 18 (a) Screen plot of eigenvalues from the unrotated principal component extraction, with cumulative variance explained; (b) Heatmap of the Varimax-rotated loadings for the three retained components (PC1 = Salinisation/mineralisation, PC2 = Alkalinity/geogenic fluoride, PC3 = Anthropogenic nitrate/pH)

Table 5. Varimax-Rotated PCA loadings for the three retained components, Jojari watershed, pre-monsoon 2025

Parameter	PC1	PC2	PC3
pH	−0.26	0.04	0.65
EC	0.81	0.48	−0.14
TDS	0.81	0.47	−0.19
TH	0.93	−0.01	0.08
Ca	0.87	−0.08	−0.25
Mg	0.76	0.04	0.40
Na	0.77	0.56	−0.12
K	0.69	0.17	0.12
Cl	0.82	0.44	−0.14
SO_4^{2-}	0.69	0.27	−0.42
HCO_3^-	0.02	0.76	0.42
NO_3^-	0.18	−0.05	0.75
F	0.21	0.70	−0.19
Variance (%)	45.08	16.55	13.06

Loadings ≥ 0.60 in absolute value are shown in bold.

5.7.3. Hierarchical Cluster Analysis

Ward's linkage HCA separates three clusters (Figure 19, Table 6). The largest jump in linkage height occurs between two and three clusters (22.3 to 15.4, against 9.3 for the next merge), and the mean silhouette width is similar for two and three clusters (0.32), which indicates a weak to moderate structure [44]; the three-cluster solution was chosen because it separates the extreme wells from the broader saline group. Cluster 1 (34 wells from all four blocks) has moderate EC (about 2,667 µS/cm), TDS (about 1,588 mg/L) and fluoride (about 1.3 mg/L) and the lower nitrate of the two larger clusters (about 77 mg/L, still above the BIS limit), with a mean WQI of 161 (Poor). It represents the evaporation-influenced but less affected baseline groundwater. Cluster 2 (4 wells, all in Luni block) is small but extreme, with EC of about 16,541 µS/cm, TDS of about 11,083 mg/L, chloride of about 4,261 mg/L, fluoride of about 5.2 mg/L, low nitrate (about 17 mg/L) and a mean WQI of 777 (Unsuitable). All four of these wells (Obs_ID 7, 13, 17 and 18) lie within 3 km of an industrial-area boundary (Section 5.9). Their chloride-rich but nitrate-poor chemistry is consistent with evaporation plus a local saline wastewater input, although a natural evaporative end-member cannot be ruled out, and this cluster is the most severe salinity hotspot in the watershed. Its high fluoride is most likely geogenic fluoride concentrated by evaporation, since fluoride shows no relationship with industrial distance (Section 5.9). Cluster 3 (21 wells from Luni, Mandore and Baori) combines high salinity (EC about 7,754 µS/cm) and high fluoride (about 4.5 mg/L) with the highest mean nitrate (about 150 mg/L) and a mean WQI of 420 (Unsuitable), a mixed signature in which sewage- or fertilizer-derived nitrate is added to evaporative salinity. As shown in Section 5.9, nitrate does not decrease towards the industrial areas; it rises slightly with distance.

Read together with the PCA, the clusters show at least three overlapping processes: a natural salinity signal from evaporation and mineral dissolution present in all clusters (PC1); a local industrial salinity signal rich in chloride near the industrial corridor (Section 5.9); and a separate nitrate signal (PC3) that lacks the distance pattern of the salinity indicators and is most likely linked to sewage or farm return flow. Similar multi-source patterns have been resolved with PCA, HCA and PMF in other urbanised basins [27, 28].

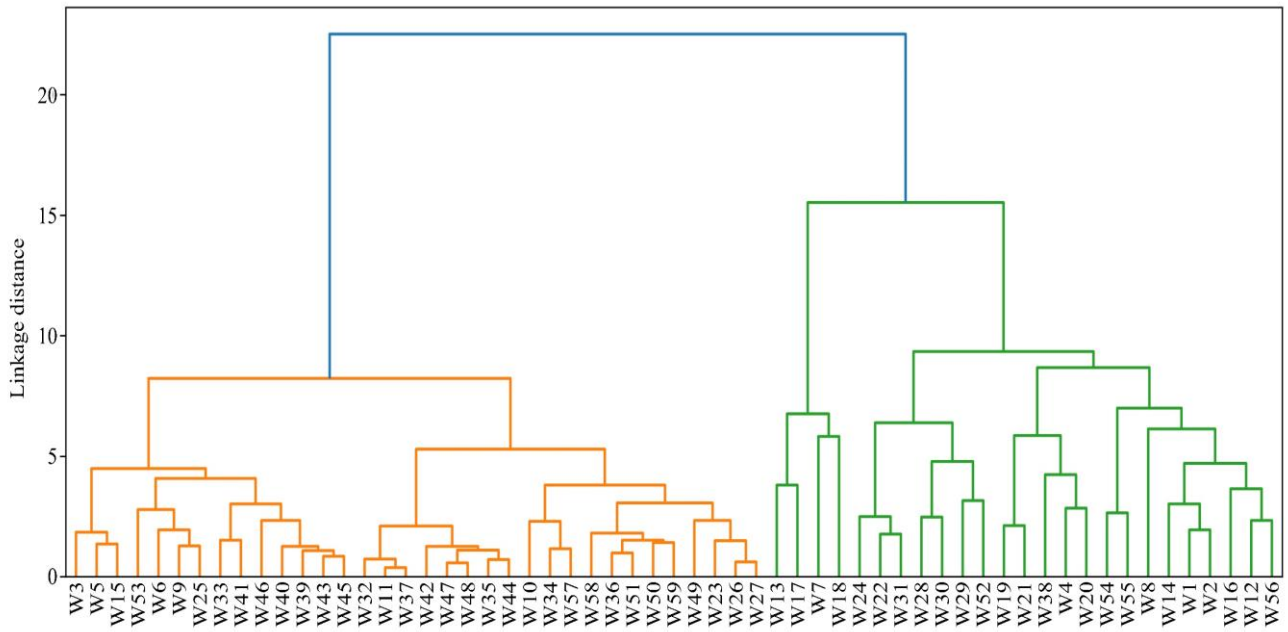


Fig. 19 Dendrogram from ward's-linkage Hierarchical Cluster Analysis (HCA) of the 59 groundwater monitoring sites

Table 6. Characteristics of the three HCA-derived hydrochemical clusters, Jojari watershed, pre-monsoon 2025

Cluster	N	Mean EC (µS/cm)	Mean TDS (mg/L)	Mean Cl (mg/L)	Mean NO_3^- (mg/L)	Mean F (mg/L)	Mean WQI (class)
1	34	2,667	1,588	568	77	1.3	161 (Poor)
2	4	16,541	11,083	4,261	17	5.2	777 (Unsuitable)
3	21	7,754	4,816	1,818	150	4.5	420 (Unsuitable)

5.8. Probable Contamination Sources

The spatial, facies, Gibbs, correlation, PCA and HCA results agree on a three-part account of groundwater deterioration, which Sections 5.9 and 5.10 then test. The first part is a natural, watershed-wide process: strong evaporation in a low-recharge arid aquifer, aided by rock–water interaction and salt dissolution. It produces the dominant Na-Cl facies, the evaporation signature on the Gibbs plots, the tight EC-TDS-Cl-Na correlation and the PC1 pattern, and on its own it can account for the moderate salinity of Cluster 1. The second part is a possible local addition near the industrial belt: the most extreme salinity values (Cluster 2) and the excess EC, TDS, Na, Cl and SO_4^{2-} near the Basni, Sangaria, Salawas and Boranada industrial areas are associated with proximity (Section 5.9), but this association is only partly robust (Section 5.10). The third part is a separate nitrate load, captured by PC3 and high in Cluster 3, most likely from farm return flow and domestic sewage across the urban and rural fringe of Jodhpur; unlike salinity, nitrate increases slightly with distance from the industrial corridor. Fluoride, captured by PC2, shows no link with industrial proximity and appears to be mainly geogenic, released by rock–water interaction in the crystalline aquifer under alkaline, bicarbonate-rich conditions, as reported for similar aquifers in India [15, 16, 19].

This source screening is qualitative. Formal apportionment of each source's share would need a coupled PCA-HCA-PMF approach [27, 28] with multi-season data and, where possible, isotope or effluent-tracer data (Section 6.1).

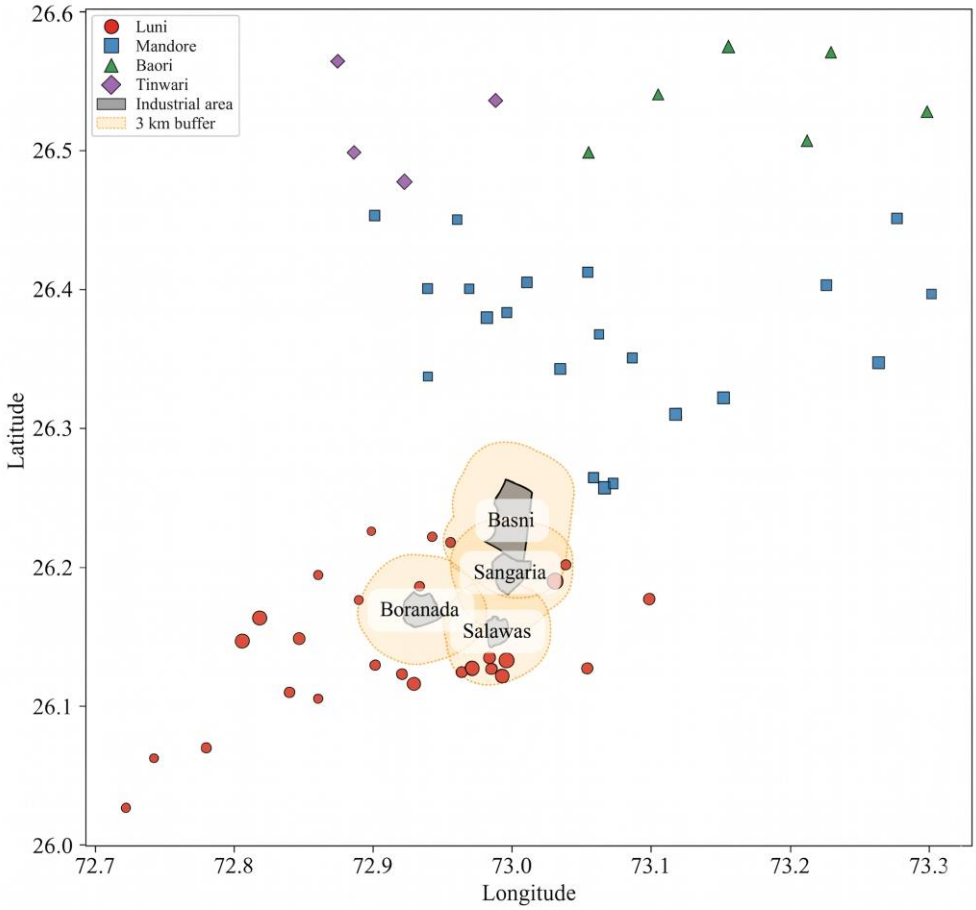


Fig. 20 Groundwater wells relative to the four industrial areas (Basni, Sangaria, Salawas and Boranada) and their 3 km buffer zones, Jojari watershed; marker size scales with Electrical Conductivity (EC)

5.9. GIS-based Proximity Analysis

The overlay of industrial-area boundaries on the maps (Section 5.2) raises a direct question: does groundwater salinity actually fall with distance from the four industrial areas? The straight-line distance from each well to the nearest industrial-area boundary was computed from the four boundary polygons (WGS 84 / UTM Zone 43N). The four areas lie close together, within about 5 km of each other, astride the Luni–Mandore block boundary (Figure 20). Distances from wells to the nearest industrial area range from 0.6 to 41.6 km (median 11.5 km). The main evidence is the continuous correlation and regression of each parameter against distance (Figure 21, Table 7), which does not depend on any cut-off. The 3 km buffer comparison is only a simple summary of that relationship. It was chosen as a practical near-corridor screening zone, not as a calibrated travel distance, and the main conclusion does not depend on the exact value of 3 km. As a check, the comparison was repeated at 2 km (5 near wells) and 5 km (17 near wells). Salinity was higher near the corridor at all three cut-offs for EC and TDS ($p < 0.05$ in every case) and for Cl^- and SO_4^{2-} at 3 km and 5 km. At 2 km, Cl^- and SO_4^{2-} were still higher near the corridor but did not reach significance ($p = 0.13$ and 0.17), which is expected with only five near wells.

Distance to the nearest industrial area shows significant negative correlations with EC ($r = -0.37$, $p = 0.004$), TDS ($r = -0.39$, $p = 0.002$), Na^+ ($r = -0.30$, $p = 0.020$), Cl^- ($r = -0.32$, $p = 0.014$) and SO_4^{2-} ($r = -0.35$, $p = 0.006$). The main salinity indicators therefore decline away from the industrial corridor, although distance alone explains only about 9–15% of their variation (r^2), as expected where evaporation sets a strong regional background. Nitrate shows a weak positive correlation with distance ($r = +0.28$, $p = 0.034$), and fluoride shows none ($r = -0.13$, $p = 0.338$). The buffer comparison agrees: the 11 wells within 3 km of an industrial boundary, all of which lie in Luni block, have mean EC, TDS, Na^+, Cl^- and SO_4^{2-} about 2.1 to 3.4 times higher than the 48 wells beyond 3 km, and the rank-based Mann–Whitney tests are significant for all five (EC ($p = 0.0007$), TDS ($p = 0.0006$), Na ($p = 0.013$), Cl ($p = 0.0046$), SO_4^{2-} ($p = 0.0028$)). Nitrate is lower inside the buffer (76.5 vs. 103.9 mg/L, $p = 0.239$), and fluoride, although higher near the corridor (4.1 vs. 2.4 mg/L), shows no significant difference ($p = 0.176$).

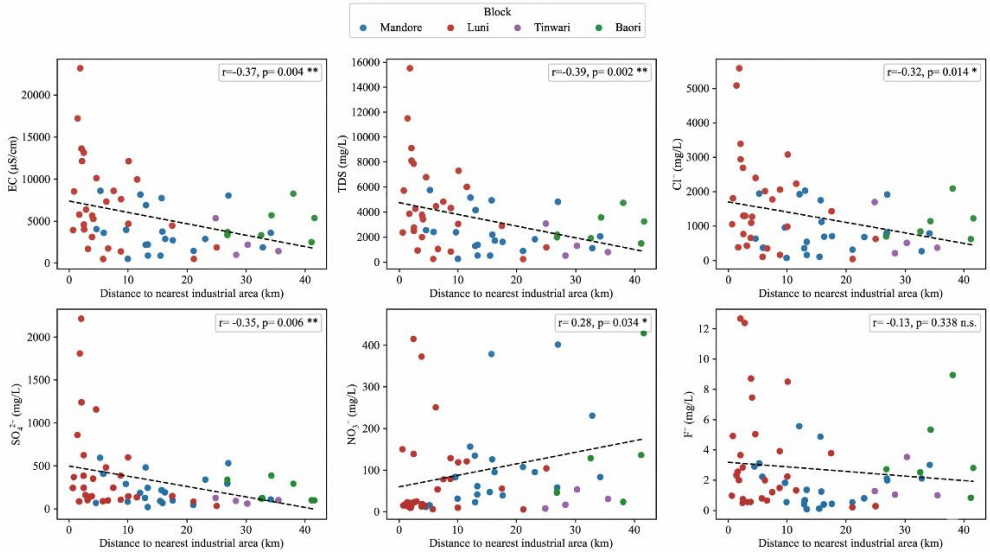


Fig. 21 Selected groundwater-quality parameters plotted against distance to the nearest industrial area, with linear regression trend lines, Jojari watershed, pre-monsoon 2025 (n = 59); ∗ ∗ p < 0.01, ∗ p < 0.05, n.s. = Not Significant; sodium statistics are given in Table 7

Table 7. Correlation between distance to the nearest industrial area and groundwater parameters, with comparison of wells within and beyond a 3 km buffer, Jojari watershed, pre-monsoon 2025

Parameter	Pearson r (vs. distance)	p-value	Near ≤ 3 km mean (n = 11)	Far > 3 km mean (n = 48)	Buffer p-value
EC (µS/cm)	−0.37	0.004	10,244	4,312	0.0007
TDS (mg/L)	−0.39	0.002	6,700	2,620	0.0006
Na (mg/L)	−0.30	0.020	1,465	687	0.013
Cl (mg/L)	−0.32	0.014	2,393	1,005	0.0046
SO_4^{2-} (mg/L)	−0.35	0.006	748	222	0.0028
NO_3^- (mg/L)	+0.28	0.034	76.5	103.9	0.239 (n.s.)
F (mg/L)	−0.13	0.338 (n.s.)	4.1	2.4	0.176 (n.s.)

n.s. = Not Significant (p > 0.05). Buffer p-values are from the Mann-Whitney U test.

Proximity to the industrial corridor is linked to the EC-TDS-Na-Cl-SO_4^{2-} indicators that load on the salinity factor (PC1), and not to nitrate (PC3). Sodium chloride and sodium sulphate are used in large amounts as electrolytes in reactive dyeing and give textile effluent its high salt load [22, 23], and comparable effluent effects on groundwater have been recorded elsewhere in the Luni basin [24, 25]. The Na–Cl–SO_4 enrichment within a few kilometres of the industrial boundaries is therefore consistent with saline industrial wastewater added to the natural salinity of the watershed. Urban sewage is a less likely explanation for this near-corridor salinity, because nitrate, its usual marker, is lower near the industrial areas than farther away. The lack of any fluoride–distance relationship supports the geogenic origin proposed for PC2. The hydrogeological evidence is less clear. Of the 11 wells within 3 km of an industrial boundary, 8 lie on the south-western side of the nearest industrial area, that is, down-gradient in the regional flow direction shown in Figure 4; but the 3 up- or cross-gradient wells (Obs_ID 6, 7 and 25) are just as saline (mean EC 10,605 µS/cm against 10,109 µS/cm), and they include the most saline well in the data set (Obs_ID 7). The near-corridor salinity therefore does not follow the expected flow direction, which argues against reading the distance pattern as a simple effluent plume. Further caution is needed. Straight-line distance ignores flow direction, aquifer heterogeneity and travel time; the analysis tests association and does not apportion sources; and the data set has no dye-specific organic compounds, industrial tracer metals, COD, colour or isotopes that could fingerprint textile effluent uniquely. The sensitivity tests in Section 5.10 show, in addition, that the association depends partly on the four Cluster 2 wells and overlaps strongly with the regional south-westward salinity gradient. The distance pattern is therefore treated as a screening signal that identifies where industrial influence is plausible and where tracer sampling should be concentrated, not as confirmation of industrial contamination.

5.10. Robustness and Sensitivity Analyses

Table 8 summarizes the sensitivity tests for data quality, the WQI, PCA and HCA. Restricting the data to the 40 samples within ±5% CBE leaves the results almost unchanged: Na-Cl water makes up 85.0% of these samples (84.7% overall), 87.5% are Poor to Unsuitable (88.1% overall), and the three PCA components are recovered with congruence coefficients of 0.997, 0.988 and 0.920. The 19 samples between ±5% and ±10% are not concentrated in the most saline wells (Spearman ρ between |CBE| and EC = 0.25, p = 0.06). The wider charge-balance limit therefore does not affect the main conclusions. The WQI classification is robust to the inclusion of correlated parameters and to the weighting scheme. Removing TDS changes the class of 10 wells, all by one class, and removing EC changes 2; with equal weights only 1 well changes class, and the share of Poor to Unsuitable wells stays between 86.4% and 88.1% in every case, with rank correlations of at least 0.993 with the original index. The choice of reference limits matters more: using BIS permissible instead of acceptable limits changes the class of 40 wells and lowers the Poor to Unsuitable share to 72.9%, which is expected because the permissible limits are two to four times higher. Even under this relaxed standard, nearly three-quarters of the wells remain unsuitable without treatment.

Table 8. Sensitivity of the main results to data screening, WQI formulation, PCA and HCA choices

Test	Result (original value in brackets where relevant)
Samples within ±5% CBE (n = 40)	Na-Cl facies 85.0% (84.7%); Poor to Unsuitable 87.5% (88.1%); PCA congruence 0.997, 0.988, 0.920
WQI without TDS	10 wells change class (all by one class); Poor to Unsuitable 86.4%; ρ = 0.993
WQI without EC	2 wells change class; Poor to Unsuitable 88.1%; ρ = 0.999
WQI with equal weights	1 well changes class; Poor to Unsuitable 88.1%; ρ = 0.995
WQI with TH acceptable limit (200 mg/L)	2 wells change class; Poor to Unsuitable 88.1%; ρ = 0.999
WQI with BIS permissible limits	40 wells change class; Poor to Unsuitable 72.9%; ρ = 0.985
PCA: parallel analysis	Only PC1 exceeds the random 95th percentile (6.78 vs 2.10); PC2 1.65 vs 1.79; PC3 1.29 vs 1.58
PCA: bootstrap (1,000)	Median congruence 0.978, 0.852, 0.841
PCA: log-transformed data	Congruence 0.996, 0.959, 0.946
PCA: without Cluster 2 wells	Congruence 0.982, 0.955, 0.894
PCA: without TDS	PC1 structure unchanged; 44.3% of variance
HCA: silhouette width	0.32 (k = 2), 0.32 (k = 3), 0.31 (k = 4)
HCA: bootstrap Jaccard	0.90, 0.79, 0.78 (Clusters 1–3)
HCA: agreement (ARI)	k-means 0.79; average or complete linkage 0.22; log-transformed 0.27

ρ = Spearman rank correlation with the original WQI. Congruence values are Tucker's coefficients for PC1, PC2 and PC3.

PC1 is highly stable: its median bootstrap congruence is 0.978, and it is recovered with congruence of 0.98 or more in every sensitivity data set. PC2 and PC3 are moderately stable, with median bootstrap congruence of 0.852 and 0.841, which corresponds to fair similarity [43]; they reappear in the log-transformed data (0.959 and 0.946), without the Cluster 2 wells (0.955 and 0.894) and in the ±5% subset (0.988 and 0.920).

Without the four extreme wells, part of the Na-Cl salinity loading moves from PC1 to the bicarbonate–fluoride component, which shows that these wells strengthen the Na-Cl character of PC1. The fluoride and nitrate factors are therefore supported, but their exact loadings should not be over-interpreted.

The HCA partition is moderately stable. The bootstrap Jaccard coefficients are 0.90, 0.79 and 0.78 for Clusters 1, 2 and 3, all above the 0.75 level usually taken to indicate a stable cluster [45], and the partition agrees well with k-means (ARI = 0.79). Agreement with average and complete linkage (ARI = 0.22) and with log-transformed data (ARI = 0.27) is lower, mainly because these methods treat the extreme wells differently: on a log scale the four Cluster 2 wells merge with the broader saline group. Cluster 2 is therefore best read as the extreme tail of the saline groundwater rather than a separate population, while the split between baseline and saline groundwater is robust.

Cross-validation of the IDW maps (Table 9) shows low predictive accuracy at unsampled locations. The observed–predicted correlations range from 0.33 to 0.46, and the RMSE is close to the standard deviation of each parameter (ratio 0.94 to 1.03), so the interpolated value at a point is little better than the watershed mean.

A power of 1 lowers the RMSE slightly (ratio 0.85 to 0.94) but does not change this conclusion. The low skill reflects strong short-range variation between neighbouring wells and the sparse network, and it confirms that the maps should be read only as broad regional patterns.

Table 9. Leave-one-out cross-validation of IDW interpolation (power 2, 12 nearest wells)

Parameter	ME	RMSE	SD	r
EC (µS/cm)	381	4,113	4,372	0.46
TDS (mg/L)	279	2,741	2,895	0.46
Cl^- (mg/L)	81	1,123	1,132	0.36
SO_4^{2-} (mg/L)	67	419	407	0.44
Na^+ (mg/L)	61	697	678	0.33
NO_3^- (mg/L)	−11	112	120	0.37
F^- (mg/L)	0.16	2.68	2.84	0.43

ME = Mean Error; RMSE = Root-Mean-Square Error; SD = Standard Deviation of observed values; r = observed–predicted correlation.

The proximity results are the least robust (Table 10). The raw associations hold under rank correlation (Spearman ρ = −0.30 to −0.43) and are not driven by any single well (leave-one-out r for EC ranges from −0.40 to −0.34). Without the four Cluster 2 wells, however, the relationship weakens: TDS remains significant (r = −0.29, p = 0.034), EC and SO_4^{2-} remain significant only by rank correlation (ρ = −0.29 and −0.28), and Na^+ and Cl^- are no longer significant; in the 3 km buffer comparison, only EC and TDS stay significant (p = 0.043). Distance to the industrial areas is also strongly collinear with regional position (R^2 = 0.62 with UTM northing), because the corridor lies in the lower part of the watershed where evaporative salinity accumulates.

After controlling for easting and northing, none of the salinity indicators is significantly related to distance (partial r = −0.07 to −0.21). Within Luni block, which removes the contrast between blocks, sulphate (ρ = −0.47, p = 0.011) and TDS (ρ = −0.39, p = 0.042) still decline with distance. Nitrate keeps its weak positive relationship with distance after controlling for location (partial r = 0.26, p = 0.047), and fluoride remains unrelated in every test.

Because all 11 near-corridor wells lie in Luni block, the industrial signal was also compared within that block. Against the other 17 Luni wells, the near-corridor wells have 2.0 times higher mean EC (10,244 vs. 5,123 µS/cm, Mann–Whitney p = 0.027), 2.1 times higher TDS (6,700 vs. 3,139 mg/L, p = 0.024) and 2.9 times higher sulphate (748 vs. 260 mg/L, p = 0.014); chloride is 2.0 times higher (2,393 vs. 1,218 mg/L) but not significantly so (p = 0.060). The industrial signal is therefore concentrated in Luni block.

Within the block, however, it also depends on the four Cluster 2 wells: without them, none of the salinity indicators is significantly related to distance (ρ = −0.31 to +0.05), and none is after controlling for location.

Table 10. Sensitivity of the distance–parameter relationships

Parameter	r (all)	ρ (all)	ρ (no Cl. 2)	Partial r	ρ (Luni)
EC	−0.37**	−0.41**	−0.29*	−0.15	−0.37
TDS	−0.39**	−0.43**	−0.31*	−0.17	−0.39*
Na^+	−0.30*	−0.30*	−0.16	−0.07	−0.24
Cl^-	−0.32*	−0.31*	−0.17	−0.11	−0.30
SO_4^{2-}	−0.35**	−0.40**	−0.28*	−0.21	−0.47*
NO_3^-	+0.28*	+0.33*	+0.25	+0.26*	+0.09
F^-	−0.13	−0.13	−0.05	+0.04	−0.19

r = Pearson; ρ = Spearman; no Cl. 2 = without the four Cluster 2 wells (n = 55); partial r controls for UTM easting and northing; Luni = Luni block only (n = 28). ∗ p < 0.05; ∗ ∗ p < 0.01.

Two conclusions follow. First, the regional salinity background, the geogenic fluoride signal and the distinct nitrate signal remain consistent across the checks. Second, the industrial-proximity signal is real in the raw data but cannot be separated from the regional salinity gradient with the present data, and it relies partly on four extreme wells. The strongest indication of industrial influence is the sulphate excess in Luni block, where near-corridor wells carry 2.9 times more sulphate than other Luni wells, because sodium sulphate is a major dyeing electrolyte [23]; even this gradient, however, depends on the Cluster 2 wells. Industrial contribution is therefore treated as probable in Luni block near the corridor, but not confirmed.

5.11. Comparison with Previous Studies

Table 11 compares the present results with earlier studies in Rajasthan and the Luni basin. Three points emerge. First, contamination in the Jojari watershed is more severe than in the Rajasthan studies compared here, although exceedance rates also depend on how wells were selected in each study. Nitrate exceeds 45 mg/L in 55.9% of wells, about twice the 28% reported for Dausa district [21], although the maximum (463.8 mg/L) is similar to the 491.6 mg/L found by Mondal et al. [1].

Fluoride exceeds 1.5 mg/L in 54.2% of wells, against about 26% in the semi-arid area studied by Mondal et al., and the maximum of 12.65 mg/L is about twice theirs. The dominance of Na^+ and Cl^- matches the semi-arid Rajasthan aquifer studied by Mondal et al. [1], and the evaporation control matches semi-arid hard-rock aquifers in southern India [19], which supports a natural origin for the regional salinity background.

Table 11. Comparison of the present results with previous groundwater studies in Rajasthan and the Luni basin

Study and area	Data and methods	Main findings	Source attribution
Mondal et al. [1], semi-arid Rajasthan	70 wells, two seasons; irrigation indices, chloro-alkaline indices	NO_3^- up to 491.6 mg/L; F^- up to 6.50 mg/L, about 26% > 1.5 mg/L; about 46% unsuitable for irrigation	Chemical weathering; nitrate from agriculture and small-scale urbanisation (qualitative)
Rahman et al. [21], Dausa district	Semi-arid district of about 3,420 km²; background-level approach	28% of samples > 45 mg/L NO_3^-; background level 7.2 mg/L	Fertilizer and human/animal waste (background exceedance)
Bhakar and Singh [14], hyper-arid Rajasthan	43 samples; PCA, HCA	Strong inter-parameter correlation; spatial grouping of wells	Statistical grouping only
Pareta et al. [10], Ayad basin, Udaipur	GWD/CGWB data 2000–2023; weighted arithmetic WQI	Quality worsens west to east; salinity main problem in east	Qualitative
Pathak et al. [25], Bandi River, Pali (Luni basin)	Effluent, river and well data 1998–2009; RS, GIS, modelling	NO_3^-, F^- and heavy metals rising in wells	Textile effluent (field and time-trend evidence)
Present study, Jojari watershed	59 wells, full major-ion suite; WQI, SAR/%Na/RSC, Piper, Gibbs, PCA, HCA, IDW, proximity test	88.1% Poor to Unsuitable WQI; 55.9% > 45 mg/L NO_3^-; 54.2% > 1.5 mg/L F^-; 85% Na–Cl	Salinity associated with industrial distance ($p \leq 0.020$) but partly confounded with the regional gradient; nitrate rises with distance; fluoride unrelated

Second, the present study tests its source interpretation more explicitly. Earlier Rajasthan studies [10-12, 14] identified salinity, nitrate and fluoride problems and grouped them under natural and anthropogenic causes without testing any source against a mapped location. Studies near industrial areas elsewhere have either attributed contaminants to industry without a distance test [31] or found weak, non-significant distance correlations and still named the plant as a main source [8]. Here, the indicators of the three PCA factors are checked against measured distance to mapped industrial boundaries: the salinity indicators decline with distance, nitrate increases slightly, and fluoride is unrelated. The sensitivity tests then show how much of this pattern survives, and they lead to a more limited conclusion than the raw correlations would suggest. The Pali studies [24, 25] showed effluent impacts along the Bandi River through field data, remote sensing and time trends; the present work adds a statistical distance test, with its limits made explicit, for a different tributary of the same basin. Third, several design choices make the results more reliable than a standard index-and-PCA assessment. The full major-ion data set allows Piper, Gibbs, SAR, %Na and RSC analysis, which is not possible with the six- or seven-parameter data sets often available for the region. The WQI classes, facies proportions and PCA structure were shown to be stable under a stricter charge-balance limit and alternative WQI formulations. The proximity test uses polygon boundaries rather than point locations of industrial areas, it was repeated at three buffer widths, and it was checked for the influence of extreme wells and regional trends. Finally, every statistical test uses measured well values rather than interpolated surfaces, which matters here because cross-validation shows that the IDW maps have little predictive skill at unsampled locations.

6. Conclusion

This study gives an integrated hydrogeochemical and geospatial assessment of groundwater in 59 wells of the Jojari River watershed, Jodhpur district, for the 2025 pre-monsoon season. The main conclusions are as follows.

1. Groundwater is mainly of Na-Cl type (about 85% of samples) and rests on a strong regional salinity background attributed mainly to evaporation and mineral dissolution under arid conditions.
2. About 88% of wells are Poor to Unsuitable for drinking by WQI, and Luni block is the most severely affected part of the watershed. Nitrate (55.9% of wells above 45 mg/L) and fluoride (54.2% above 1.5 mg/L) are the main health concerns.
3. For irrigation, most samples carry high to very high salinity hazard (USSL C3-C4), while carbonate hazard by RSC is limited.
4. PCA (74.7% of variance) and HCA resolve a regional salinity factor, a nitrate factor most likely linked to fertilizer-bearing farm return flow and sewage, and a mainly geogenic fluoride factor.
5. EC, TDS, Na, Cl and SO_4^{2-} decline with distance from the Basni–Sangaria–Salawas–Boranada corridor ($p \leq 0.020$), and wells within 3 km of an industrial boundary have about 2.1 to 3.4 times higher mean values of these indicators. Nitrate rises slightly with distance ($r = +0.28$), and fluoride shows no relationship. The salinity association weakens without the four Cluster 2 wells and cannot be separated from the regional south-westward salinity gradient; the industrial signal is concentrated in Luni block, where the 11 near-corridor wells have 2.0–2.9 times higher EC, TDS and sulphate than other Luni wells. A local industrial contribution there is probable but not confirmed, and it is not quantified as a share of total salinity.

Testing statistical source signals against measured distance from mapped industrial boundaries, together with explicit robustness checks, offers a simple and repeatable screening step for arid industrial basins. In this study, the checks were decisive: they separated the robust findings (the regional salinity background, the geogenic fluoride signal and the distinct nitrate signal) from the weaker industrial-proximity signal, and they show that tracer data are needed before industrial contribution can be quantified.

The extreme hotspot formed by HCA Cluster 2 in Luni block (Obs_ID 7, 13, 17 and 18) calls for a specific monitoring and regulatory response rather than general advice. The following framework is proposed for that zone.

Sentinel Monitoring Network

The four Cluster 2 wells should be designated as sentinel wells, with additional monitoring wells placed down-gradient (south-west, following Figure 4) of the Sangaria and Salawas industrial areas. Sampling should be at least quarterly and should cover EC, TDS, Na^+, Cl^-, SO_4^{2-}, F^- and NO_3^- together with effluent tracers such as COD, colour, boron and heavy metals (Cr, Cu, Zn and Pb), so that industrial inputs can be fingerprinted.

Action Levels

BIS permissible limits (for example, Cl^- above 1,000 mg/L or TDS above 2,000 mg/L), or a rise of more than an agreed margin over each sentinel well's baseline between two rounds, should trigger inspection of the effluent treatment and discharge records of the nearest industrial units and Common Effluent Treatment Plants (CETPs).

Source Control

CETPs serving the four industrial areas should be held to their zero-liquid-discharge or discharge consents, with online continuous effluent monitoring at CETP outlets and public reporting, in line with the Critically Polluted Industrial Cluster action plan [3]. Sentinel-well results should also be reported publicly and to the Rajasthan State Pollution Control Board.

Protection of Drinking Supply

Untreated groundwater from the hotspot should not be used for drinking. Piped surface-water supply, or community reverse-osmosis and defluoridation units with safe disposal of reject brine, should be provided, and new drinking-water abstraction in the zone should be restricted under the aquifer-management framework of the CGWB [34].

Irrigation Management

In C3-C4 zones of Luni and Baori blocks, salt-tolerant crops, gypsum application, leaching and blending with better-quality water are advised.

Outside the hotspot, the separate nitrate signal (PC3, Cluster 3) needs control of domestic sewage and fertilizer use, and the geogenic fluoride (PC2) needs defluoridation or alternative supply rather than industrial regulation.

6.1. Limitations and Future Work

The study rests on a single pre-monsoon sampling round in 2025. Without post-monsoon data, seasonal dilution and flushing of salts after recharge cannot be assessed, and persistent contamination cannot be separated from seasonal change; this is an important constraint for shallow alluvial and weathered hard-rock aquifers, and the results should be read as a pre-monsoon baseline. Post-monsoon sampling of the same wells is the first planned extension. The data are secondary records compiled from three agencies, so laboratory quality control could not be verified beyond the internal consistency checks reported here, and well coverage is uneven, with only six wells in Baori and four in Tinwari. The proximity analysis uses straight-line distance and does not account for hydraulic gradient, flow direction or aquifer heterogeneity; distance is also strongly collinear with regional position, which the present design cannot resolve. A calibrated groundwater flow and transport model (for example MODFLOW and MT3DMS), building on hydrodynamic work on the Jojari channel [26], would replace straight-line distance with flow-path distance and travel time, while heavy-metal, dye-specific organic, COD and isotope data would allow textile effluent to be fingerprinted directly. Finally, the relative shares of evaporation, industrial effluent, farm return flow and sewage could be estimated with a coupled PCA-HCA-PMF or isotope-tracer framework [27, 28].

Conflicts of Interest

The author(s) declare(s) that there is no conflict of interest regarding the publication of this paper.

Funding Statement

This research did not receive any specific grant from funding agencies in the public, commercial, or not-for-profit sectors.

Acknowledgments

The authors thank the Ground Water Department, Rajasthan, the Central Ground Water Board and the Rajasthan State Pollution Control Board for access to groundwater-quality monitoring records.

References

[1] N. C. Mondal et al., "A Diagnosis of Groundwater Quality from a Semiarid Region in Rajasthan, India," *Arabian Journal of Geosciences*, vol. 9, no. 12, 2016. [CrossRef] [Google Scholar] [Publisher Link]

[2] Surindra Suthar et al., "Nitrate Contamination in Groundwater of Some Rural Areas of Rajasthan, India," *Journal of Hazardous Materials*, vol. 171, no. 1-3, pp. 189-199, 2009. [CrossRef] [Google Scholar] [Publisher Link]

[3] Comprehensive Environmental Pollution Abatement Action Plan for Critically Polluted Industrial Cluster - Jodhpur, Rajasthan State Pollution Control Board, Jaipur, India, 2020. [Online]. Available: https://environment.rajasthan.gov.in/content/dam/environment/RPCB/CEPIactionplans/CEPI_Action%20Plan_Jodhpur.pdf

[4] Santosh Yadav, Sangeeta Parihar, and Sandeep Yadav, "Industrial Wastewater Management in Western Rajasthan: Current Practices, Environmental Impacts and Sustainable Solutions," *Sustainable Chemistry One World*, vol. 7, 2025. [CrossRef] [Google Scholar] [Publisher Link]

[5] "*IS 10500:2012: Indian Standard Drinking Water - Specification*," Bureau of Indian Standards, pp. 1-18, 2012. [Google Scholar] [Publisher Link]

[6] Arthur M. Piper, "A Graphic Procedure in the Geochemical Interpretation of Water-Analyses," *Eos, Transactions American Geophysical Union*, vol. 25, no. 6, pp. 914-928, 1944. [CrossRef] [Google Scholar] [Publisher Link]

[7] Ronald J. Gibbs, "Mechanisms Controlling World Water Chemistry," *Science*, vol. 170, no. 3962, pp. 1088-1090, 1970. [CrossRef] [Google Scholar] [Publisher Link]

[8] Abbas Ali Zamani, Mohammad Reza Yaftian, and Abdolhossein Parizanganeh, "Multivariate Statistical Assessment of Heavy Metal Pollution Sources of Groundwater around a Lead and Zinc Plant," *Iranian Journal of Environmental Health Science & Engineering*, vol. 9, no. 1, pp. 1-10, 2012. [CrossRef] [Google Scholar] [Publisher Link]

[9] K. Alagulakshmi et al., "Spatio-Temporal Patterns of Land Use and Land Cover, and their Impact on Groundwater Quality in the Industrialized Muvattupuzha Basin," *Scientific Reports*, vol. 15, pp. 1-25, 2025. [CrossRef] [Google Scholar] [Publisher Link]

[10] Kuldeep Pareta et al., "Groundwater Quality Assessment for Drinking and Irrigation Purposes in the Ayad River Basin, Udaipur (India)," *Groundwater for Sustainable Development*, vol. 27, pp. 1-20, 2024. [CrossRef] [Google Scholar] [Publisher Link]

[11] Vinay Kumar Gautam et al., "Groundwater Quality Characterization using an Integrated Water Quality Index and Multivariate Statistical Techniques," *PLOS One*, vol. 19, no. 2, pp. 1-23, 2024. [CrossRef] [Google Scholar] [Publisher Link]

[12] Sangeeta Choudhary et al., "Assessing Sources of Groundwater Quality and Health Risks using Graphical, Multivariate, and Index Techniques from a Part of Rajasthan, India," *Groundwater for Sustainable Development*, vol. 27, 2024. [CrossRef] [Google Scholar] [Publisher Link]

[13] Deepesh Machiwal, and Madan K. Jha, "Identifying Sources of Groundwater Contamination in a Hard-Rock Aquifer System Using Multivariate Statistical Analyses and GIS-Based Geostatistical Modeling Techniques," *Journal of Hydrology: Regional Studies*, vol. 4, pp. 80-110, 2015. [CrossRef] [Google Scholar] [Publisher Link]

[14] Prashant Bhakar, and Ajit Pratap Singh, "Groundwater Quality Assessment in a Hyper-Arid Region of Rajasthan, India," *Natural Resources Research*, vol. 28, no. 2, pp. 505-522, 2019. [CrossRef] [Google Scholar] [Publisher Link]

[15] Baru Ram et al., "Geogenic Controls on Groundwater Chemistry and Drinking Water Quality Index (DWQI) Evaluation in Semi-Arid Mahendragarh District, Haryana," *Cleaner Water*, vol. 5, pp. 1-11, 2026. [CrossRef] [Google Scholar] [Publisher Link]

[16] Somvir Singh, N. C. Mondal, and Surendra Kaur Rawal, "Assessment of Groundwater Quality for Drinking and Irrigation Purposes Using Water Quality Index and Statistical Analysis in Nalanda District, South Bihar, India," *Discover Environment*, vol. 4, no. 1, pp. 1-31, 2026. [CrossRef] [Google Scholar] [Publisher Link]

[17] Gurugnanam Balasubramaniyan et al., "Spatial Assessment of Groundwater Potability and Irrigation Suitability using Water Quality Index and Geospatial Analysis in Natham Taluk, Tamil Nadu, India," *Discover Sustainability*, vol. 7, no. 1, pp. 1-26, 2026. [CrossRef] [Google Scholar] [Publisher Link]

[18] Kuldeep Tiwari, Rohit Goyal, and Archana Sarkar, "GIS-based Spatial Distribution of Groundwater Quality and Regional Suitability Evaluation for Drinking Water," *Environmental Processes*, vol. 4, no. 3, pp. 645-662, 2017. [CrossRef] [Google Scholar] [Publisher Link]

[19] Anbarasu Subramaniyan, "Geogenic and Anthropogenic Controls on Water Quality and Associated Health Risks in the Hard Rock, Southern India," *Environmental Science and Pollution Research*, vol. 33, no. 10, pp. 4130-4147, 2026. [CrossRef] [Google Scholar] [Publisher Link]

[20] Sangeeta Parihar et al., "Geochemical Assessment of Groundwater Quality using Nemerov's Pollution Index: A Micro-Level Study in the Groundwater Critical Zone of Western Rajasthan, India," *Journal of Water and Health*, vol. 23, no. 1, pp. 16-25, 2025. [CrossRef] [Google Scholar] [Publisher Link]

[21] Abdur Rahman, N.C. Mondal, and K.K. Tiwari, "Anthropogenic Nitrate in Groundwater and its Health Risks in the View of Background Concentration in a Semi Arid Area of Rajasthan, India," *Scientific Reports*, vol. 11, pp. 1-13, 2021. [CrossRef] [Google Scholar] [Publisher Link]

[22] Rita Kant, "Textile Dyeing Industry an Environmental Hazard," *Natural Science*, vol. 4, no. 1, pp. 22-26, 2012. [CrossRef] [Google Scholar] [Publisher Link]

[23] Awais Khatri et al., "A Review on Developments in Dyeing Cotton Fabrics with Reactive Dyes for Reducing Effluent Pollution," *Journal of Cleaner Production*, vol. 87, pp. 50-57, 2015. [CrossRef] [Google Scholar] [Publisher Link]

[24] B.K. Bhadra, Suparn Pathak, and J.R. Sharma, "Impact of Industrial Effluents on Groundwater around Pali City, Rajasthan Using Field and Satellite Data," *Journal of the Geological Society of India*, vol. 82, no. 6, pp. 675-691, 2013. [CrossRef] [Google Scholar] [Publisher Link]

[25] S. Pathak, B.K. Bhadra, and J.R. Sharma, "Study of Influence of Effluent on Ground Water using Remote Sensing, GIS and Modeling Techniques," *The International Archives of the Photogrammetry, Remote Sensing and Spatial Information Sciences*, vol. XXXIX-B4, pp. 345-348, 2012. [CrossRef] [Google Scholar] [Publisher Link]

[26] Aman Meena et al., "MIKE 2D-Hydrodynamic Modelling of the Jojari River: Spatio-Temporal Analysis of Flow, Inundation, and Anthropogenic Influences (2015–2020)," *Environment, Development and Sustainability*, 2026. [CrossRef] [Google Scholar] [Publisher Link]

[27] Anjali Bhagwat, and Prasad Ojha, "Statistical Ensemble for Groundwater Pollution Source Identification and Quantification of Source Contribution," *Journal of Environmental Engineering*, vol. 152, no. 2, pp. 1-12, 2025. [CrossRef] [Google Scholar] [Publisher Link]

[28] Xiao Li et al., "Groundwater Pollution Source Identification based on a Coupled PCA–PMF–Mantel Framework: A Case Study of the Qujiang River Basin," *Water*, vol. 17, no. 19, pp. 1-21, 2025. [CrossRef] [Google Scholar] [Publisher Link]

[29] Jin Li, and Andrew D. Heap, "A Review of Comparative Studies of Spatial Interpolation Methods in Environmental Sciences: Performance and Impact Factors," *Ecological Informatics*, vol. 6, no. 3-4, pp. 228-241, 2011. [CrossRef] [Google Scholar] [Publisher Link]

[30] Gordon Gong, Sravan Mattevada, and Sid E. O'Bryant, "Comparison of the Accuracy of Kriging and IDW Interpolations in Estimating Groundwater Arsenic Concentrations in Texas," *Environmental Research*, vol. 130, pp. 59-69, 2014. [CrossRef] [Google Scholar] [Publisher Link]

[31] A. Keshav Krishna, K. Rama Mohan, and B. Dasaram, "Assessment of Groundwater Quality, Toxicity and Health Risk in an Industrial area using Multivariate Statistical Methods," *Environmental Systems Research*, vol. 8, no. 1, pp. 1-17, 2019. [CrossRef] [Google Scholar] [Publisher Link]

[32] Krishna Kumar Yadav et al., "GIS-based Evaluation of Groundwater Geochemistry and Statistical Determination of the Fate of Contaminants in Shallow Aquifers from Different Functional Areas of Agra City, India: Levels and Spatial Distributions," *RSC Advances*, vol. 8, no. 29, pp. 15876-15889, 2018. [CrossRef] [Google Scholar] [Publisher Link]

[33] Philip J. Clark, and Francis C. Evans, "Distance to Nearest Neighbor as a Measure of Spatial Relationships in Populations," *Ecology*, vol. 35, no. 4, pp. 445-453, 1954. [CrossRef] [Google Scholar] [Publisher Link]

[34] "*NAQUIM 2.0 Studies in Jodhpur Urban Agglomerates, Jodhpur District of Rajasthan State AAP 2023-24*," Central Ground Water Board, Ministry of Jal Shakti, Government of India, 2024. [Google Scholar] [Publisher Link]

[35] American Public Health Association, *Standard Methods for the Examination of Water and Wastewater*, 23rd ed., APHA, pp. 1-40, 2017. [Google Scholar] [Publisher Link]

[36] R. Allan Freeze, and John A. Cherry, *Groundwater*, Prentice-Hall, pp. 1-604, 1979. [Google Scholar] [Publisher Link]

[37] Steven J. Fritz, "A Survey of Charge-Balance Errors on Published Analyses of Potable Ground and Surface Waters," *Groundwater*, vol. 32, no. 4, pp. 539-546, 1994. [CrossRef] [Google Scholar] [Publisher Link]

[38] Chandra Bhushan et al., "Hydrogeochemical Characterisation and Human Health Risk Assessment of Groundwater in Sultanpur District, Uttar Pradesh, India," *Frontiers in Water*, vol. 7, pp. 1-24, 2025. [CrossRef] [Google Scholar] [Publisher Link]

[39] *Guidelines for Drinking-Water Quality, 4th ed., Incorporating the 1st Addendum*, World Health Organization, pp. 1-541, 2017. [Google Scholar] [Publisher Link]

[40] L.A. Richards, *Diagnosis and Improvement of Saline and Alkali Soils*, US Government Printing Office, pp. 1-160, 1954. [Google Scholar] [Publisher Link]

[41] L.V. Wilcox, *Classification and Use of Irrigation Waters*, United States Department of Agriculture, pp. 1-19, 1955. [Google Scholar] [Publisher Link]

[42] John L. Horn, "A Rationale and Test for the Number of Factors in Factor Analysis," *Psychometrika*, vol. 30, no. 2, pp. 179-185, 1965. [CrossRef] [Google Scholar] [Publisher Link]

[43] Urbano Lorenzo-Seva, and Jos M.F. Ten Berge, "Tucker's Congruence Coefficient as a Meaningful Index of Factor Similarity," *Methodology*, vol. 2, no. 2, pp. 57-64, 2006. [CrossRef] [Google Scholar] [Publisher Link]

[44] Peter J. Rousseeuw, "Silhouettes: A Graphical Aid to the Interpretation and Validation of Cluster Analysis," *Journal of Computational and Applied Mathematics*, vol. 20, pp. 53-65, 1987. [CrossRef] [Google Scholar] [Publisher Link]

[45] Christian Hennig, "Cluster-wise Assessment of Cluster Stability," *Computational Statistics & Data Analysis*, vol. 52, no. 1, pp. 258-271, 2007. [CrossRef] [Google Scholar] [Publisher Link]

[46] R. Webster, and M.A. Oliver, "Sample Adequately to Estimate Variograms of Soil Properties," *Journal of Soil Science*, vol. 43, no. 1, pp. 177-192, 1992. [CrossRef] [Google Scholar] [Publisher Link]